DEHN SURGERIES ON 2-BRIDGE LINKS WHICH YIELD REDUCIBLE 3-MANIFOLDS

HIROSHI GODA, CHUICHIRO HAYASHI AND HYUN-JONG SONG

1. Introduction

No surgery on a non-torus 2-bridge knot yields a reducible 3-manifold as shown in Theorem 2(a) in [7] by A. Hatcher and W. Thurston. Dehn surgeries on 2-bridge knots are already well studied by M. Brittenham and Y.-Q. Wu in [2]. See also [11].

On 2-bridge links of 2-components, Wu showed in [13, Theorem 5.1 and Remark 5.5] the following theorem. The universal covering space of a laminar 3-manifold M is the Euclidean 3-space $\mathbb{R}^3$, and then M is not reducible by [4].

Theorem 1.1. ([13]) *A non-trivial Dehn surgery on a 2-bridge link yields a laminar 3-manifold except for the 2-bridge links $L([r,s])$ with $[r,s] = 1/(r+1/s)$. For them with $r, s \neq \pm 1$, we obtain laminar 3-manifolds if the two surgery slopes are both non-integral.*

In this paper we study Dehn surgery on 2-bridge links $L([r,s])$. Note that $L([r,s])$ is a link of 2-components if and only if both r and s are odd integers. Since $L([r,s]) \cong L([-s,-r])$ and $L([-r,-s]) \cong L([s,r])$ is the mirror image of $L([r,s])$, it is enough to consider $L([r,s])$ with $r > 0$. When $|r| = 1$ or $|s| = 1$, $L([r,s])$ is a $(2,k)$-torus link for some even integer k. Thus we consider the case where $r \geq 3$ and either $s \geq 3$ or $s \leq -3$.

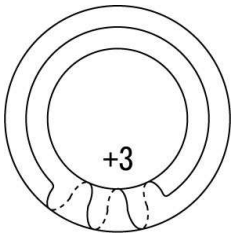

Figure 1.

Every component of a 2-bridge link is the trivial knot. We coordinate slopes on the toral boundaries of the link exterior so that the slope in Figure 1 is $+3$ rather than -3. Let

This work was supported by Joint Research Project 'Geometric and Algebraic Aspects of Knot Theory', under the Japan-Korea Basic Scientific Cooperation Program by KOSEF and JSPS. The authors would like to thank Professor Hitoshi Murakami for giving us this opportunity. The first and second authors are partially supported by Grant-in-Aid for Scientific Research, (No. 15740031 and No. 15740047 respectively), Ministry of Education, Science, Sports and Technology, Japan.

$L(p/q)[\gamma_1, \gamma_2]$ be the 3-manifold obtained by the Dehn surgery on the 2-bridge link $L(p/q)$ with surgery slopes γ_1 and γ_2. The order of the surgery slopes γ_1, γ_2 is not crucial since every 2-bridge links has a symmetry of π-rotation which exchanges the two components. See Figure 2.

Theorem 1.2. *$L([2w+1, 2u+1])[\gamma_1, \gamma_2]$ with $w \geq 1$ and either $u \geq 1$ or $u \leq -2$ is a reducible 3-manifold if and only if it is one of the followings or its mirror image.*

(1) (a) *$\gamma_1 = -w + u + 1$ and $\gamma_2 = -w + u - 1$.*
    (b) *$\gamma_1 = -w + u$ and $\gamma_2 = -w + u$.*
(2) *$w = 1$, $u = -2$ and $\gamma_1 = -1$ and $\gamma_2 = -6$.*

If we perform Dehn surgery of slope γ on one component of a 2-bridge link $L(p/q)$, then the other component forms a knot in a lens space, $S^1 \times S^2$ or S^3. We denote it by $L(p/q)[\gamma]$. The next two theorems show when it is a torus knot or a cable knot in S^3. More general version on knots in lens spaces is given in Theorem 11.1.

Theorem 1.3. *Let $L(p/q)$ be a non-torus 2-bridge link. Then $L(p/q)[\gamma]$ is a non-trivial torus knot in S^3 if and only if it is one of the followings or its mirror image.*

(1) *$p/q = [p+2, p]$, $\gamma = 1$ and $L(p/q)[\gamma]$ is the $(p, -(p+2))$-torus knot.*
(2) *$p/q = [3, 3]$, $\gamma = 1$ and $L(p/q)[\gamma]$ is the $(2, -5)$-torus knot.*
(3) *$p/q = [-3, 3]$, $\gamma = -1$ and $L(p/q)[\gamma]$ is the $(2, -3)$-torus knot.*

Theorem 1.4. *Let $L(p/q)$ be a non-torus 2-bridge link. Then $L(p/q)[\gamma]$ is a cable knot in S^3 if and only if it is one of the followings or its mirror image.*

(1) *When $w = u$, $L([2w+1, 2u+1])[1]$ is the $(2, -2w^2-2w-1)$-cable of the $(w, -w-1)$-torus knot.*
(2) *When $w = u + 2$, $L([2w+1, 2u+1])[-1]$ is the $(2, 2w^2 - 2w - 1)$-cable of the $(-w, -w+1)$-torus knot.*

Remark 1.5.

(1) Theorem 1.3 (1) gives counter examples for Ait-Nouh and Yasuhara's conjecture: if a (p, q)-torus knot ($q \geq p > 0$) is obtained by a twisting operation on the trivial knot, then $q = np \pm 1$ for some integer n. See [1]. The existence of the counter examples has already been shown in the previous paper [5].
(2) The essential planar surface corresponding to Theorem 1.2 (3) has 4 boundary circles of slope -1 on a component of the link, and 2 boundary circles of slope -6 on the other component. See Calculation for d_{26} in Section 10. This shows that the cabling conjecture for hyperbolic knots in S^3 can not be extended to those in a lens space. Because $L([3, -3])[-6]$ is a hyperbolic knot in the $(6, -1)$-lens space according to the computer software SnapPea programmed by J. Weeks.

(3) $L([3,3])[\pm 1]$ is the $(2, \mp 5)$-torus knot as shown in Theorem 1.3 (2). Note that $L([3,3])$ is amphicheiral.

In general, let M be a 3-manifold, and K a knot in the interior of M. Then K is called a *composite knot* if there is a 2-sphere S intersecting K transversely in two points in M such that S does not bound a 3-ball which K intersects in a trivial arc. Otherwise, K is called a *prime knot*. We say that K is a *satellite knot* if its exterior E contains an incompressible torus which is not parallel to a toral boundary component of E.

Theorem 1.6. *Suppose $L(p/q)$ is a non-torus 2-bridge link. If $L(p/q)[\gamma]$ is a prime satellite knot, then either (1) $L(p/q) \cong L([2w+1, 2u+1])$ for some integer w, u with $w \geq 2$ and either $u \geq 2$ or $u \leq -3$, and $\gamma = -w + u \pm 1$, or (2) $L(p/q) \cong L([2w, v, 2u])$ for some integers w, v, u with $|w|, |v|, |u| \geq 2$. Conversely, in case (1), $L([2w+1, 2u+1])(-w+u\pm 1)$ is a satellite knot.*

In fact, in case (1), it is a cable knot of a torus knot in the $(-w + u \pm 1, 1)$-lens space by Theorem 11.1.

It is well-known that, if $L(p/q)[\gamma_1, \gamma_2]$ is reducible, then the exterior of $L(p/q)$ contains an essential planar surface with boundary slopes γ_i on $\partial N(L_i)$ for $i = 1$ and 2, where "essential" means incompressible and boundary incompressible.

Our study is based on the classification of essential surfaces in 2-bridge link exteriors by W. Floyd and A. Hatcher ([3]). We assume the readers' good familiarity with their study. The space of isotopy classes of the surfaces is much more complicated than that of 2-bridge knot ([7]). A. Lash gives a way to calculation of boundary slopes for such surfaces, and did calculate for the Whitehead link $L([3,-3])$ in [9]. We should note that J.Hoste and P.Shanahan [8] improved the way of Lash recently. However, the way of calculation of genera of the surfaces is not given there. Note that the surfaces carried by branched surfaces given in [3] may be non-orientable or disconnected.

This paper is organized as follows. In Section 2, we recall results in [3], [9]. In Section 3, we obtain all the minimal edge-paths for $L([r,s])$. In Section 5, we give a way to calculate Euler characteristics of such surfaces. In Section 6, we generalize the notion of genus for disconnected or non-orientable surfaces. The generalized genus is zero if and only if there is either a planar component or a projective plane with holes component. In Section 7 and 8, we calculate boundary slopes, Euler characteristics, generalized genus of the surfaces carried by the branched surfaces corresponding to certain two minimal paths. In Section 9, we give data of all the essential surfaces in the exterior of $L([r,s])$. In Section 10 and Appendix A, the proof of "only if part" of Theorem 1.2 is given. In Section 11, we give the proofs of sufficiency of Theorems 1.2, 1.3, 1.4 and 11.1. In Section 12, we prove Theorem 1.6.

2. A summary of results of Floyd, Hatcher and Lash

W. Floyd and A. E. Hatcher studied the spaces of incompressible surfaces in 2-bridge link exteriors in [3]. A. E. Lash studied the way how to compute the spaces of boundary slopes of incompressible surfaces for 2-bridge links in Chapter 1 in his doctoral dissertation [9]. (He calculated the space of boundary slopes for the Whitehead link $L([3,-3])$.)

In this section, we briefly recall their results. Very roughly speaking, every orientable essential surface is carried by a branched surface corresponding to a minimal edge-path in a certain planar graph in the upper half plane, as below.

The diagrams of slope system and minimal edge-paths.

The diagram D_1 is an embedded graph on the upper half plane $\mathbb{H}$ with the real line $\mathbb{R}$ and the point at infinity $1/0$ such that its vertices are the rational points in $\mathbb{R}\cup\{1/0\}$ and that its edges are geodesics on the upper half model of the hyperbolic plane and join two vertices a/c, b/d if and only if $ad-bc=\pm 1$. We regard the vertex 0 as $0/1$. See Figure 1.1 in [3], where the diagram D_1 transformed onto the Poincaré disc model by $-\dfrac{z-\frac{1+i}{2}}{z-\frac{1-i}{2}}$ is described. (Figure 4 in [7] is transformed by $-\dfrac{z-i}{z+i}$.)

We identify the matrix $\begin{pmatrix} a & b \\ c & d \end{pmatrix} \in PSL_2\mathbb{R}$ with the Möbius transformation $\dfrac{az+b}{cz+d}$, an orientation preserving isometry of the upper half model of the hyperbolic plane. Let $G\subset PSL_2(\mathbb{Z})$ be the subgroup of transformations $\begin{pmatrix} a & b \\ c & d \end{pmatrix}$ with c being an even integer. G-images of the ideal quadrilateral $\langle 0/1, 1/0, 1/1, 1/2\rangle$ form a tiling of the upper half plane by quadrilaterals. These edges form the G-orbit of the edge $\langle 1/0, 0/1\rangle$ and we label them by A. The other edges of D_1 are diagonals of the quadrilaterals and form the G-orbit of the edge $\langle 0/1, 1/1\rangle$. We label them by C.

We form the diagram $D_0 = D_\infty$ from D_1 by deleting all the edges labeled C and adding the G-orbit of the edge $\langle 1/0, 1/2\rangle$. The new edges are the opposite diagonals of the quadrilaterals, and we label them by D. The edges of the quadrilaterals are labeled by B in the diagram $D_0 = D_\infty$.

For $0 < t < \infty$ with $t \neq 1$, the diagram D_t is obtained from D_1 by deleting the diagonal edge labeled C in each quadrilateral Q and adding a small rectangle having a vertex in the interior of each edge of Q so that $g(D_t) = D_t$ for arbitral $g \in G$. (We distinguish these small rectangles from the quadrilaterals by keeping to call them rectangles rather than quadrilaterals, to avoid confusion.) The edge $\langle 1/0, 0/1\rangle$ is divided to two edges by the added vertex. We label by A the G-orbit of one of them including the vertex $1/0$, and that of the other including $0/1$ by B. We label by C (resp. D) an edge of an added small

rectangle if it cobounds a triangle face together with two edges with label A (resp. B). The edges of D_t is fall into four G-orbits corresponding to these four labels.

For a given reduced rational number p/q, an oriented edge-path λ from $1/0$ to p/q in D_t with $0 \leq t \leq \infty$ is called *minimal* if no two consecutive edges of λ lie in the boundary of the same triangle face or rectangle face of D_t. There is a unique finite sequence of quadrilaterals $Q_{p/q}$ such that the first one contains the vertex $1/0$, that the last one contains the vertex p/q, and that every pair of consecutive ones intersect in a single edge. Every minimal edge-path from $1/0$ to p/q is entirely contained in $Q_{p/q}$. Hence there are only finitely many such paths for p/q.

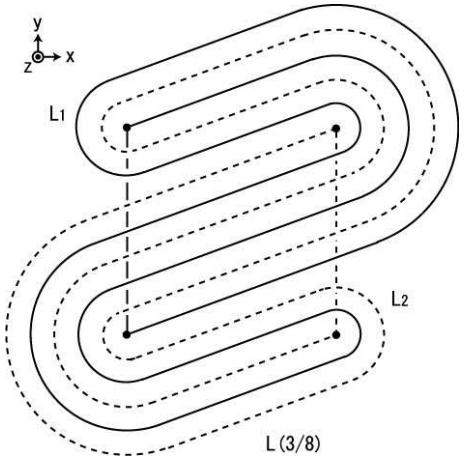

FIGURE 2.

Links and branched surfaces.

The 3-sphere S^3 can be regarded as the 2-points compactification of $S^2 \times \mathbb{R}$, and each level sphere $S^2 \times \{r\}$ as the quotient $\mathbb{R}^2/\Gamma$, where Γ is the group generated by 180° rotations about integer points in $\mathbb{R}^2$. The Γ image of a subset $S \subset \mathbb{R}^2$ is denoted by $\Gamma(S)$. Then such an S^2 has precisely four integer points $\Gamma(0,0)$, $\Gamma(1,0)$, $\Gamma(0,1)$ and $\Gamma(1,1)$. For a reduced fraction p/q with $p, q \in \mathbb{Z}$, the 2-bridge link $L(p/q)$ can be placed in $S^2 \times [0,1]$ so that (1) $L(p/q) \cap (S^2 \times \{0\})$ is the union of the two arcs of slope ∞ with their endpoints in the integer points, (2) $L(p/q) \cap (S^2 \times \{r\})$, $r \in (0,1)$ consists of the four integer points and (3) $L(p/q) \cap (S^2 \times \{1\})$ is the union of the two arcs of slope p/q with their endpoints in the integer points. In $S^2 = \mathbb{R}^2/\Gamma$ with the four integral points, the slope of the arcs are determined by the slopes of the preimage lines in $\mathbb{R}^2$. $L(p/q)$ is a 2-component link rather than a knot if and only if q is an even integer. This positioning shows that $L(p/q)$ has a symmetry by the 180° rotation about the axis $\Gamma(1/2, 1/2) \times [0,1]$, which exchanges the two components of $L(p/q)$. See Figure 2.

$SL_2(\mathbb{Z})$ acts on $\mathbb{R}^2$ by $\begin{pmatrix} a & b \\ c & d \end{pmatrix}\begin{pmatrix} y \\ x \end{pmatrix} = \begin{pmatrix} ay+bx \\ cy+dx \end{pmatrix}$. (This act is in a little unusual manner because we write the first coordinate under the second in the above two 2-dimensional vectors.) Hence $PSL_2(\mathbb{Z})$ acts on the level sphere $S^2 \times \{r\} = \mathbb{R}^2/\Gamma$. $\begin{pmatrix} a & b \\ c & d \end{pmatrix}$ brings the slope p/q to the slope $\dfrac{ap+bq}{cp+dq}$, corresponding to the Möbius transformation $\dfrac{az+b}{cz+d}$ on the upper half plane.

The vertices of the diagrams $D_1, D_0 = D_\infty, D_t$ correspond to the slopes of arcs in the level spheres. For every minimal edge-path γ in D_t with $1 < t < \infty$, we construct a corresponding branched surface Σ_γ as below. Let $e_1, \ldots, e_k$ be the sequence of edges of γ. For each edge e_i, the sub-branched surface $\Sigma_{e_i} = \Sigma_\gamma \cap (S^2 \times [(i-1)/k, i/k])$ is an adequate transformation of the branched surface $\Sigma_A, \Sigma_B, \Sigma_C, \Sigma_D$ in Figure 3.1 in [3] according to the label of e_i. (In the figure, we can find the four strand $\Gamma(0,0), \Gamma(1,0), \Gamma(0,1), \Gamma(1,1)$ of a link from the left to the right.) Precisely, $\Sigma_A, \Sigma_B, \Sigma_C, \Sigma_D$ is the branched surface corresponding to the edges A_0, B_0, C_0, D_0 as below. A_0 is oriented from $1/0$ to the interior point of $\langle 1/0, 0/1\rangle$, B_0 from $0/1$ to the interior point of $\langle 1/0, 0/1\rangle$, C_0 from the interior point of $\langle 1/0, 1/1\rangle$ to the interior point of $\langle 1/0, 0/1\rangle$ and D_0 from the interior point of $\langle 0/1, 1/2\rangle$ to the interior point of $\langle 1/0, 0/1\rangle$. (In fact, the arcs at the bottom of Σ_A are of slope $1/0$ and the arcs at the top of Σ_A are of slopes $0/1$ and $1/0$.) There is a Möbius transformation $g \in G$ with $e_i = g(e_0)$, $e_0 \in \{A_0, B_0, C_0, D_0\}$ according to the label of e_i. If the orientations of e_i and $g(e_0)$ match, then $\Sigma_{e_i} = (g \times *)\Sigma_{e_0}$, where $*$ is the map $[0,1] \ni s \mapsto (i+s-1)/k \in [(i-1)/k, i/k]$. If the orientations don't match, we reflect Σ_{e_i} upside down. Rotating Σ_γ by 180° about $\Gamma(1/2, 1/2) \times [0,1]$, we obtain the branched surface for $D_{1/t}$, where $0 < 1/t < 1$.

The diagram D_∞ has only edges labeled B and edges labeled D. We obtain Σ_B, Σ_D for D_∞ from Σ_B, Σ_D in Figure 3.1 in [3] by deleting square sectors (arcs of slope 0) $\times [0,1]$ labeled β. The resulting Σ_B (resp. Σ_D) corresponds to the edge from $0/1$ to $1/0$ (resp. from $1/2$ to $1/0$). Rotating Σ_B, Σ_D for D_∞ by 180° about $\Gamma(1/2, 1/2) \times [0,1]$, we obtain those for D_0.

The edges of D_1 are labeled A or C. We obtain Σ_A for D_1 from Σ_A in Figure 3.1 in [3] by deleting the square (the arc of slope $1/0$) $\times [1/2, 1]$ labeled $\alpha - \beta$. The resulting Σ_A corresponds to the edge from $1/0$ to $0/1$. Σ_C for D_1 is obtained from Σ_A for D_1 by transformed by $\begin{pmatrix} 1 & 0 \\ 1 & 1 \end{pmatrix}$. This corresponds to the edge from $1/1$ to $0/1$. (Σ_C for D_1 is obtained also from Σ_C in Figure 3.1 in [3] by deleting the square (the arc of slope $1/0$) $\times [0,1]$ labeled $\alpha - \beta$ and adding a complementary horizontal square of the horizontal square in the level sphere $S^2 \times \{1/2\}$.)

Then the branched surfaces for $D_0 = D_\infty$ and D_1 are constructed similarly as those for D_t with $0 < t < \infty$, $t \neq 1$.

Let L_1 (resp. L_2) be the component of $L(p/q)$ containing the arcs $\Gamma(0,0) \times [0,1]$ called strand 1 and strand 2 $\Gamma(0,1) \times [0,1]$ (resp. strand 3 $\Gamma(1,0) \times [0,1]$ and strand 4 $\Gamma(1,1) \times [0,1]$). For a surface F in the exterior of $L(p/q)$, let α (resp. β) be the minimal number of intersection points of the boundary circles $\partial F \cap \partial N(L_1)$ (resp. $\partial F \cap \partial N(L_2)$) and a meridian circle of $\partial N(L_1)$. Then $t = \alpha/\beta$, which is the subscript of D_t with $0 \leq t \leq \infty$. Suppose that F is carried by a branched surface Σ_γ as above. In Figure 3.1 in [3], where $1 < t < \infty$ and $\alpha > \beta$, the labels β, $\alpha - \beta$, $(\alpha - \beta)/2$, n, $\beta - n$ and $\alpha - \beta - n$ indicates the number of sheets carried by the sectors. The branching number n is determined for each segment Σ_{e_i} by F. $0 \leq n \leq \beta$ for Σ_A and $0 \leq n \leq \alpha - \beta$ for Σ_D when $1 \leq t \leq \infty$.

As shown in Theorem 3.1 (a) in [3], every "essential" surface in the exterior of $L(p/q)$ is carried by some branched surface corresponding to a minimal edge-path from $1/0$ to p/q in D_t with $t = \alpha/\beta$. Conversely, an orientable surface carried by such a branched surface is essential. There, an *essential* surface is an incompressible and meridionally incompressible surface without peripheral component. (We don't need to consider meridionally incompressibility because a surface with non-meridional boundary slope both on $\partial N(L_1)$ and $\partial N(L_2)$ is always meridionally incompressible.)

However, such a branched surface may carry non-orientable or disconnected surfaces. (Moreover, there may be an essential non-orientable surface which is not carried by any branched surface as above.)

Boundary slopes.

A. E. Lash calculated the space of boundary slopes for the Whitehead link in [9]. We briefly recall his tactics here. We calculate boundary slopes of surfaces with respect to the meridian μ_i and a non-standard longitude λ_i of L_i. We take λ_1 as below. In $S^2 = \mathbb{R}^2/\Gamma$, we take the arc s of slope 0 connecting $\Gamma(0,0)$ and $\Gamma(0,1)$. λ_1 is the union of the arc $(s \times [0,1]) \cap \partial N(L_1)$ and an arc in $(S^2 \times [1,\infty)) \cap \partial N(L_1)$. λ_1 is oriented toward increasing $r \in [0,1]$ along the axis $\Gamma(0,0) \times [0,1]$, and hence toward decreasing along the axis $\Gamma(0,1) \times [0,1]$. The meridian μ_1 is oriented as a right-handed circle around the axis $\Gamma(0,0) \times [0,1]$ oriented upward. We obtain λ_2, μ_2 from λ_1, μ_1 by rotating by 180° about the axis $\Gamma(1/2,1/2) \times [0,1]$. (Under this coordination, the preferred longitude of $L([r,s])$ is of slope $(1, \frac{r-s}{2})$ for both components when $s > 0$, as is shown in section 7. It is $(1, \frac{r-s}{2} - 2)$ when $s < 0$, as is shown in section 8.)

Let i_j be the algebraic intersection number $\partial F \cdot \lambda_j$ in $\partial N(L_i)$. For $1 < t \leq \infty$, $\partial \Sigma_{e_i} = \partial(g \times *)(\Sigma_{e_0})$, $g = \begin{pmatrix} a & b \\ c & d \end{pmatrix} \in G$ contributes to the number i_j as in Table 2.1 (Table 1.2 in [9]) if the orientations of e_i and $g(e_0)$ agree. If they disagree, we change all the sign of the number in Table 2.1. (If λ_i is not transverse to $\partial \Sigma_{e_i}$ for some i, we isotope whole of λ_i very

slightly to the right in $\partial N(L_i)$.) Fortunately, Table 2.1 does not depend on the branching number n. For $t = \infty$, we substitute 0 for β in Table 2.1.

label	condition on g	i_1	i_2
A	$-\infty < -\frac{d}{c} < 0$	β	β
	$0 < -\frac{d}{c} < \infty$	$-\beta$	$-\beta$
	$-\frac{d}{c} = 0, \pm\infty$	0	0
B	$-\infty < -\frac{d}{c} < 0$	$-(\alpha-\beta)$	0
	$0 < -\frac{d}{c} < \infty$	$\alpha-\beta$	0
	$-\frac{d}{c} = 0, \pm\infty$	0	0
C	$0 < -\frac{d}{c} < 1$	-2β	0
	$-\frac{d}{c} = 0, 1$	$-\beta$	β
	otherwise	0	2β
D	$\frac{1}{2} < -\frac{d}{c} < \infty$	$\alpha-\beta$	$\alpha-\beta$
	$-\frac{d}{c} = \frac{1}{2}, \pm\infty$	0	$\alpha-\beta$
	otherwise	$-(\alpha-\beta)$	$\alpha-\beta$

Table 2.1

For $0 \leq t < 1$, we interchange the column for i_1 and that for i_2 and interchange α and β in Table 2.1. For $t = 0$, we further substitute 0 for α.

For $t = 1$, contribution of $\Sigma_{e_i} = (g \times *)\Sigma_A$ to i_1, i_2 is the same as Table 2.1. Σ_C corresponds to the edge from 1/1 to 0/1, and $\Sigma_C = (\begin{pmatrix} 1 & 0 \\ 1 & 1 \end{pmatrix} \times id)\Sigma_A$. Hence, for an edge e_i labeled by C, $\partial\Sigma_{e_i} = \partial g(\Sigma_C)$ with $g = \begin{pmatrix} a & b \\ c & d \end{pmatrix} \in G$ contributes i_1 and i_2 as in Table 2.2 (Table 1.3 in [9]). We should note that it depends on n.

	condition on g	i_1	i_2
C	$-\frac{d}{c} = 0, 1$	$\beta - 2n$	$-(\beta-2n)$
	$0 < -\frac{d}{c} < 1$	$-2n$	$-2(\beta-n)$
	otherwise	$2(\beta-n)$	$2n$

Table 2.2

In the remainder of this section, we recall the way how we obtain Tables 2.1 and 2.2. We consider, for example, the case where $1 < t < \infty$ and $e_i = g(D_0)$, $g \in G$ with orientations match. Set $g = \begin{pmatrix} a & b \\ c & d \end{pmatrix}$. Then g brings the slope $-\frac{d}{c}$ to 1/0 since $\begin{pmatrix} a & b \\ c & d \end{pmatrix}\begin{pmatrix} -d \\ c \end{pmatrix} = \begin{pmatrix} -ad+bc \\ 0 \end{pmatrix} = \begin{pmatrix} -1 \\ 0 \end{pmatrix}$. Hence the intersection number between $\partial\Sigma_{e_i}$ and λ_j is equal to

that between $\partial\Sigma_D$ and the vertical line segment $(\rho \times [0,1]) \cap \partial N(L_j)$ where ρ is the arc of slope $-\dfrac{d}{c}$ in $S^2 = \mathbb{R}^2/\Gamma$.

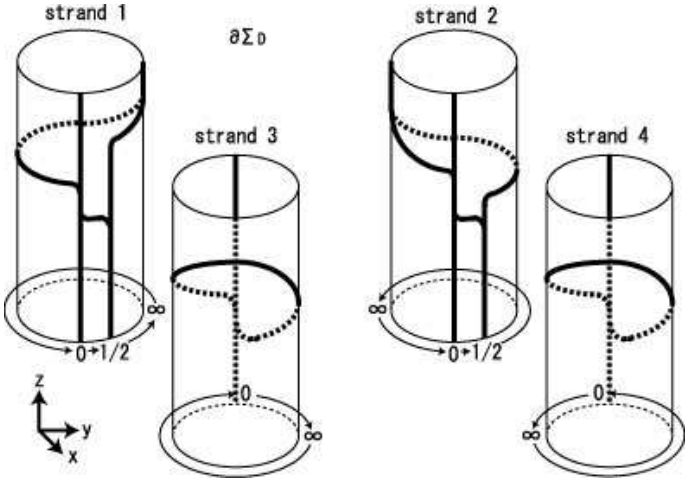

FIGURE 3.

In Figure 3, we can find $\partial\Sigma_D$. We orient $\partial\Sigma_\gamma$ so that it runs along the strands $\Gamma(0,0) \times [0,1]$ and $\Gamma(1,1) \times [0,1]$ to point upward. Figure 4 depicts the tubes about the four strands lifted into $\mathbb{R}^2 \times [0,1]$ via Γ.

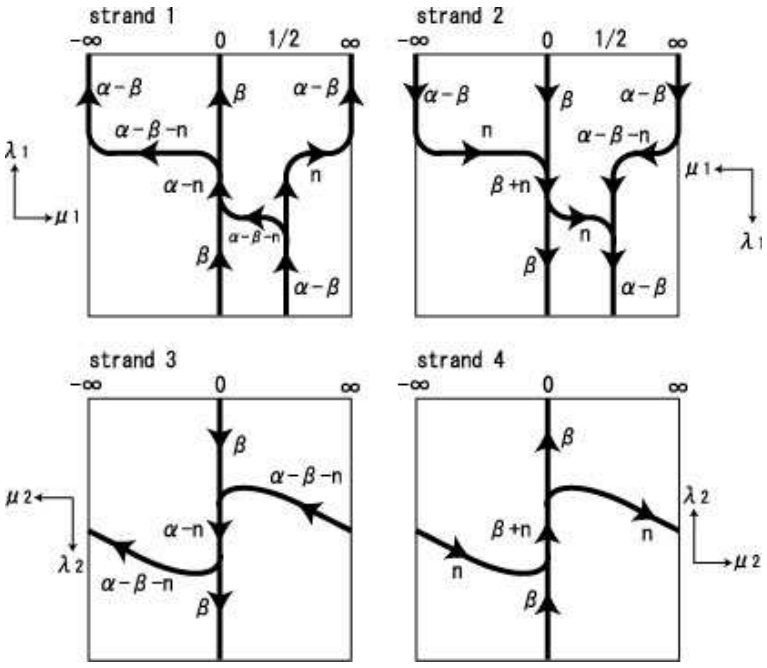

FIGURE 4.

We take the algebraic sum of these signed crossing points, to obtain Table 2.3 below. Note that λ_j points downward along strand 2 $\Gamma(0,1) \times [0,1]$ and strand 3 $\Gamma(1,0) \times [0,1]$.

We should recall that, if λ_j is not transverse to $\partial\Sigma_{e_i}$, then λ_j is isotoped slightly to the direction of orientation of μ_j if λ_j is not transverse to $\partial\Sigma_{e_i}$. Then we take sum of the intersection numbers on strands 1 and 2, and those on strands 3 and 4, to obtain the bottom three rows in Table 2.1.

label	conditionon$g$	i_1, strand1	i_1, strand2	i_2, strand3	i_2, strand4
D	$\frac{1}{2} < -\frac{d}{c} < \infty$	n	$\alpha-\beta-n$	$\alpha-\beta-n$	n
	$-\frac{d}{c} = \frac{1}{2}$	n	$-n$	$\alpha-\beta-n$	n
	$-\frac{d}{c} = \infty$	$-(\alpha-\beta-n)$	$\alpha-\beta-n$	$\alpha-\beta-n$	n
	otherwise	$-(\alpha-\beta-n)$	$-n$	$\alpha-\beta-n$	n

Table 2.3

3. Minimal edge paths

In this section we list all the minimal edge-paths for $L(p/q)$ with $p/q = [r,s] = 1/(r+1/s)$, $r = 2w+1$, $s = 2u+1$, $r \geq 3$ and $s \neq \pm 1$. Since $L(p/q) = L([r,s])$ and $L(-p/q) = L([-r,-s])$ are mirror images of each other, we can assume $r > 0$.

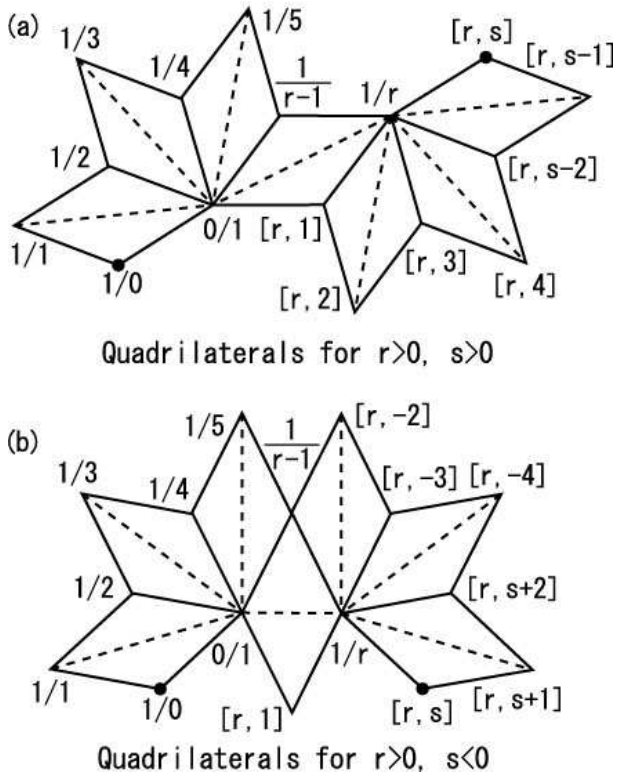

Figure 5.

The case of $s > 0$.

We consider the case of $u \geq 1$. Then $Q_{p/q}$ is a union of the sequence of $w+1$ quadrilaterals around the vertex $0/1$, and the sequence of $u+1$ quadrilaterals around the vertex $1/r$. See Figure 5 (a). The first sequence is composed of the quadrilaterals $\langle 0/1, 1/0, 1/1, 1/2\rangle$, $\langle 0/1, 1/2, 1/3, 1/4\rangle, \cdots, \langle 0/1, 1/(2i-2), 1/(2i-1), 1/2i\rangle, \cdots, \langle 0/1, 1/(r-1), 1/r, 1/(r+1)\rangle$ The last sequence is the union of the quadrilaterals $\langle 1/r, [r,-1], [r,0], [r,1]\rangle$, $\langle 1/r, [r,1], [r,2], [r,3]\rangle$, $\cdots$, $\langle 1/r, [r,2i-1], [r,2i], [r,2i+1]\rangle$, $\cdots$, $\langle 1/r, [r,s-2], [r,s-1], [r,s]\rangle$. Since $[r,0] = 1/(r+1/0) = 1/\infty = 0 = 0/1$, the last quadrilateral of the first sequence is the first one of the last sequence. Hence $Q_{p/q}$ consists of $w+u+1$ quadrilaterals.

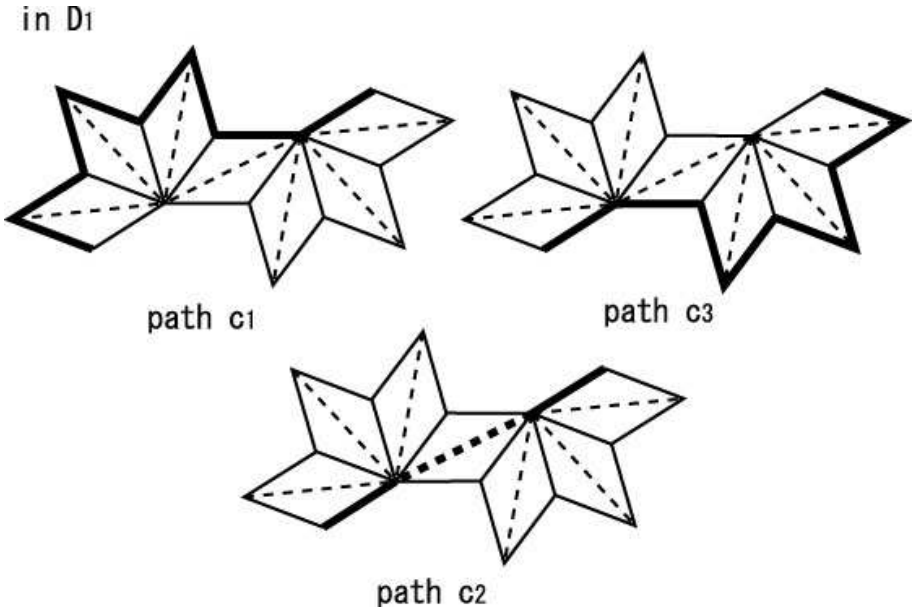

FIGURE 6.

For the diagram D_1, we have 3 minimal edge paths. See Figure 6.

The edge-path c_1 is a sequence of $2w+2$ A-edges. The first $2w$ edges connect the vertices 1/0-1/1-1/2-1/3-...-$1/(r-1)$, and the last 2 edges connect $1/(r-1)$-$1/r$-$[r,s]$.

The edge-path c_2 is a sequence of 3 edges. The first A-edge connects $1/0$ and $0/1$, the second C-edge connects $0/1$ and $1/r$ and the last A-edge connects $1/r$ and $[r,s]$.

The edge-path c_3 is a sequence of $2u+2$ A-edges. π-rotation of c_3 on the paper is c_1 in $Q_{[s,r]}$.

For the diagram $D_0 = D_\infty$, we have 5 minimal edge-paths. See Figure 7.

The edge-path c_4 is a union of 2 sequence of edges. The first sequence of w D-edges connect 1/0-1/2-1/4-1/6-...-$1/(2w) = 1/(r-1)$. The second is a sequence of 2 B-edges connecting $1/(r-1)$-$1/r$-$[r,s]$.

The edge-path c_5 is the union of 4 B-edges connecting 1/0-0/1-$1/(r-1)$-$1/r$-$[r,s]$. This edge-path is not minimal when $r=3$ ($w=1$).

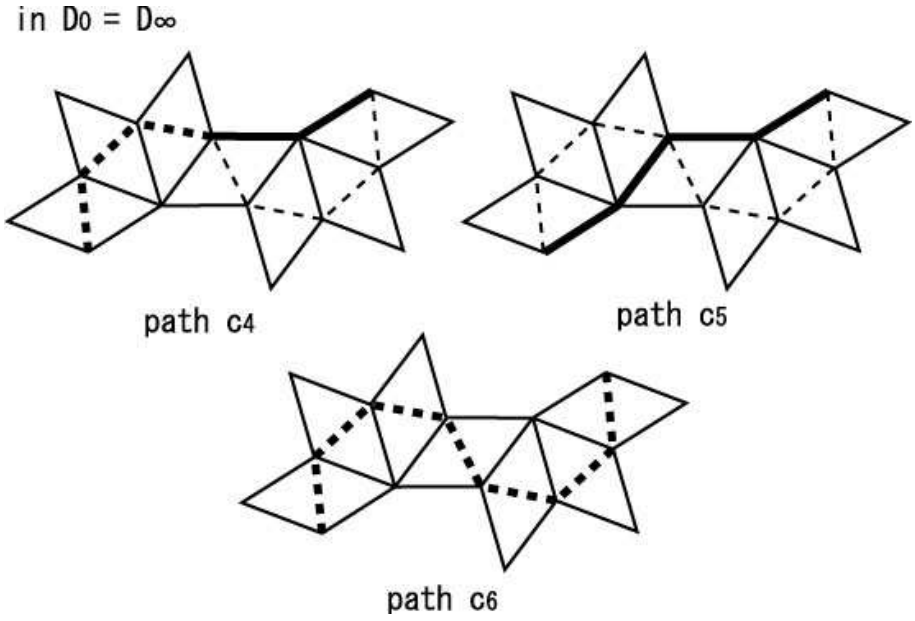

FIGURE 7.

The edge-path c_6 is a union of $w+u+1$ D-edges. The first t edges connect 1/0-1/2-1/4-1/6-...-$1/(2w) = 1/(r-1)$. The middle edge connect $1/(r-1)$-$1/(r+1)$. The last u edges connect $1/(r+1)$-$[r,3]$-...-$[r,s]$.

The edge-paths c_7 and c_8 correspond to the edge-paths c_5 and c_4 respectively by the π-rotation on the paper.

For the diagram D_t with $t \neq 0, 1, \infty$, we have 8 minimal edge-paths. See Figure 8. The edge-path c_{ij} is a "chimera" of c_i and c_j.

The edge-path c_{14} is composed of 2 sequences of edges. The first is the sequence of w triples of A-, D-, A-edges together connecting the vertices 1/0-1/2-1/4-...-$1/(2w) = 1/(r-1)$. These edges are away from the vertex 0/1. The last is the sequence of 4 A-, B-, B-, A-edges, connecting $1/(r-1)$-$1/r$-$1/[r,s]$.

The edge-path c_{16} is a union of 2 sequences of edges. The first is the same as that of c_{14}. The last is the sequence of an A-edge, $u+1$ D-edges and an A-edge together connecting $1/(r-1)$ to $[r,s]$ near the vertex $1/r$.

The edge-path c_{24} is a union of 2 sequences of edges. The first is the sequence of A-, w D-, C-, B-edges connecting 1/0-$1/r$, where the D-edges are near the vertex 0/1. The last consists of a B-edge and an A-edge connecting $1/r$ to $[r,s]$.

The edge-path c_{25} is the union of 7 edges which are A-, B-, B-, C-, B-, B-, A-edges connecting 1/0-0/1-$1/r$-$[r,s]$. The C-edge is contained in the quadrilateral $\langle 0/1, 1/(r-1), 1/r, 1/(r+1)\rangle$ and near the vertex $1/(r-1)$ rather than $1/(r+1)$. This edge-path is not minimal when $r = 3$ $(t = 1)$.

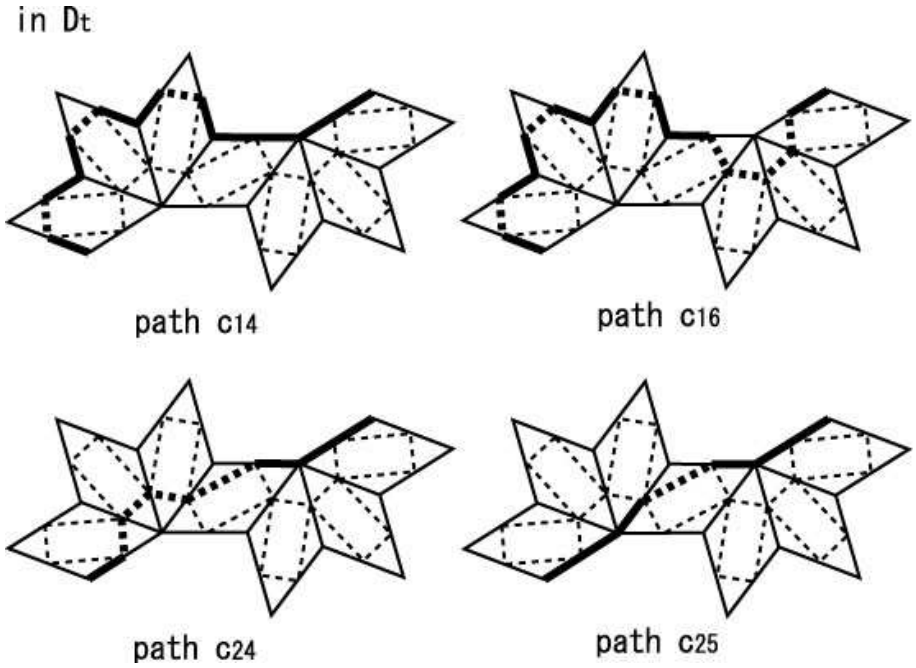

FIGURE 8.

The edge-paths c_{38}, c_{36}, c_{28}, c_{27} correspond to the edge-paths c_{14}, c_{16}, c_{24}, c_{25} respectively by the π-rotation.

The case of $s < 0$.

We set $s = 2u+1 = -(2u'+1)$. Then $u \leq -2$ and $u' \geq 1$. The sequence of quadrilaterals $Q_{p/q}$ is the union of the 2 sequences of quadrilaterals below. See Figure 5 (b). The first sequence is the precisely same one as that for $s > 0$, and is composed of $w+1$ quadrilateral. The last sequence consists of $u'+1$ quadrilaterals around the vertex $1/r$. Precisely, it is the union of the quadrilaterals $\langle 1/r, [r,1], [r,0], [r,-1]\rangle$, $\langle 1/r, [r,-1], [r,-2], [r,-3]\rangle$, $\cdots$ $\langle 1/r, [r,-2i+3], [r,-2i+2], [r,-2i+1]\rangle$, $\cdots$ $\langle 1/r, [r,s+2], [r,s+1], [r,s]\rangle$. Thus $Q_{p/q}$ consists of $w+u'+1 = w-u$ quadrilaterals.

For the diagram D_1, we have 4 minimal edge-paths. See Figure 9.

The edge-path d_0 is a union of 2 sequences of edges. The first is the sequence of $2w$ A-edges connecting 1/0-1/1-1/2-1/3-1/4-1/5-...-1/$(r-1)$. The last is the sequence of $2u'$ A-edges connecting $1/(r-1) = [r,-1]$-$[r,-2]$-$[r,-3]$-...-$[r,s]$. Thus the edge-path consists of $2w+2u'$ edges.

The edge-paths d_1, d_2 and d_3 are similar to c_1, c_2 and c_3 for $s > 0$. The edge-path d_3 corresponds to the edge-path d_1 for $Q_{[-s,-r]}$ by reflection on a vertical axis on the paper.

For the diagram $D_0 = D_\infty$, we have 5 minimal edge-paths. See Figure 10.

The edge-paths d_4, d_5, d_6, d_7 and d_8 are similar to c_4, c_5, c_6, c_7 and c_8 for $s > 0$. But, when $r = 3$ $(w = 1)$, d_5 and d_8 are not minimal. d_4 and d_5 are not minimal when $s = -3$

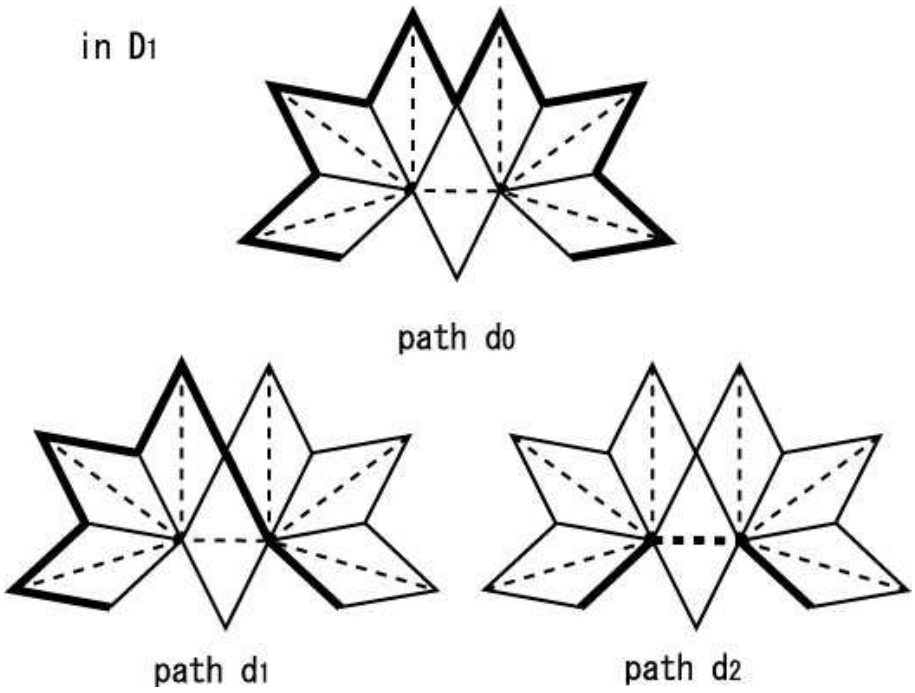

FIGURE 9.

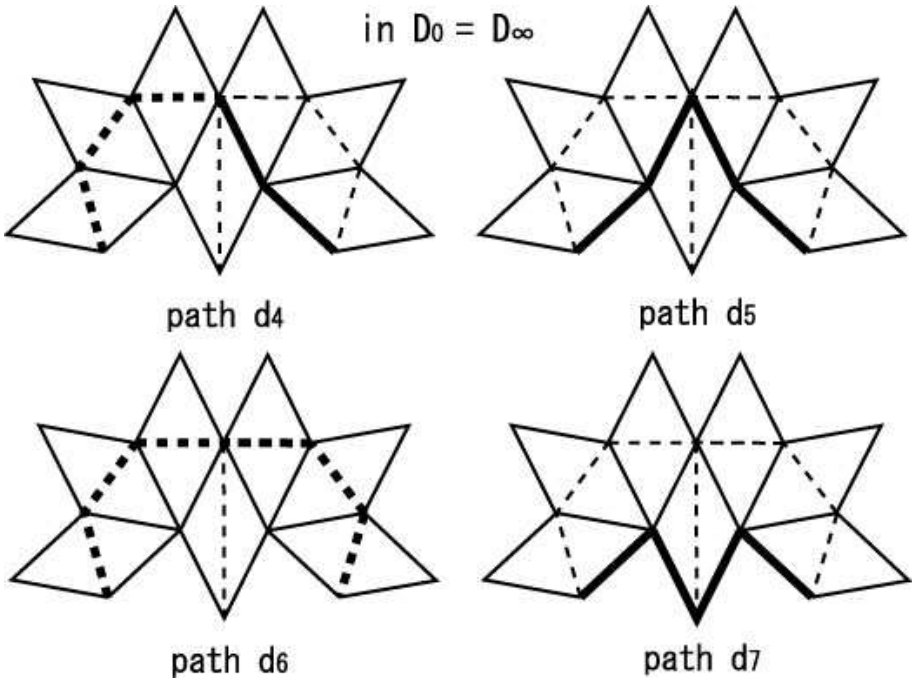

FIGURE 10.

($u' = 1$, $u = -2$). (Note that c_7 is minimal even when $r = 3$ or $s = -3$.) By reflection on a vertical axis, d_8 corresponds to d_4 for $Q_{[-s,-r]}$, while d_7 does not correspond to d_5.

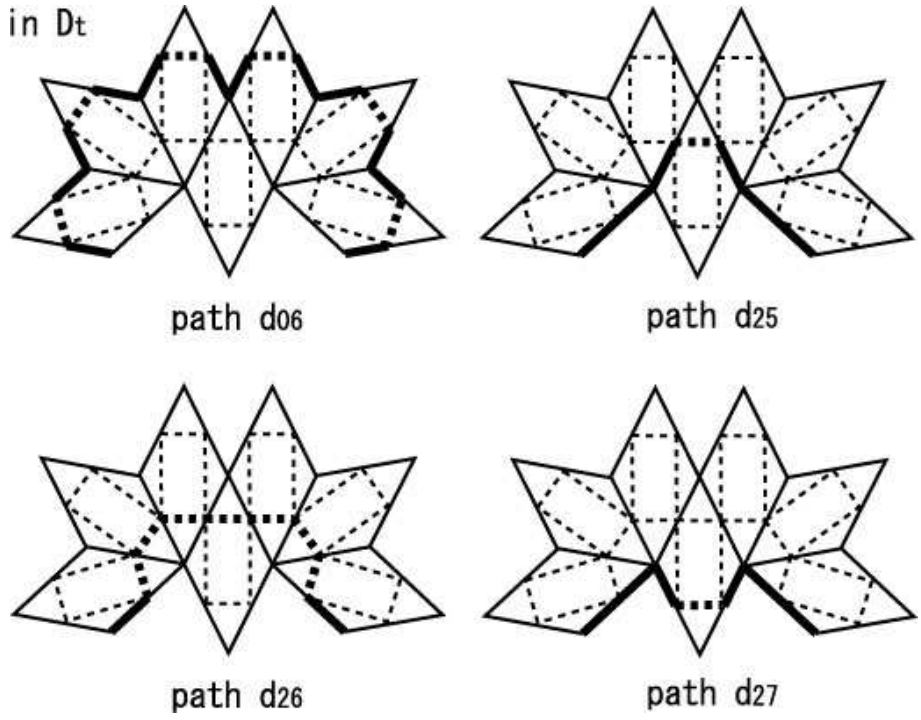

FIGURE 11.

For the diagram D_t with $t \neq 0, 1, \infty$, we have 10 minimal edge paths. See Figures 11 and 12.

The edge-path d_{06} is a union of 2 sequences of edges. The first is the sequence of w A-, D-, A-edges connecting 1/0-1/2-1/4-...-1/$(2w)$ = $1/(r-1)$ away from the vertex 0/1. The last is the sequence of u' A-, D-, A-edges connecting $[r,-1]$-$[r,-3]$-$[r,-5]$-...-$[r,s]$ away from the vertex $1/r$. Hence this edge-path consists of $3(w+u')$ edges.

The edge-path d_{26} is a sequence of an A-edge, w D-edges, a C-edge, u' D-edges and an A-edge. The first sequence of w D-edges are near the vertex 0/1, and the last ones are near $1/r$.

For the other 8 edge-paths d_{14}, d_{16}, d_{24}, d_{25}, d_{38}, d_{36}, d_{28}, d_{27}, each d_{ij} is similar to c_{ij} for $s > 0$. d_{ij} is minimal if and only if d_j is minimal.

4. TRANSFORMATION $g \in G$ WITH $e_i = g(e_0)$ AND INTERSECTION NUMBER

For $E \in \{A, B, C, D\}$, the edges E'_i in Figure 13 are the images of E_0 under the following transformations.

For the i-th quadrilateral in the first sequence of quadrilaterals $Q_{p/q}$,

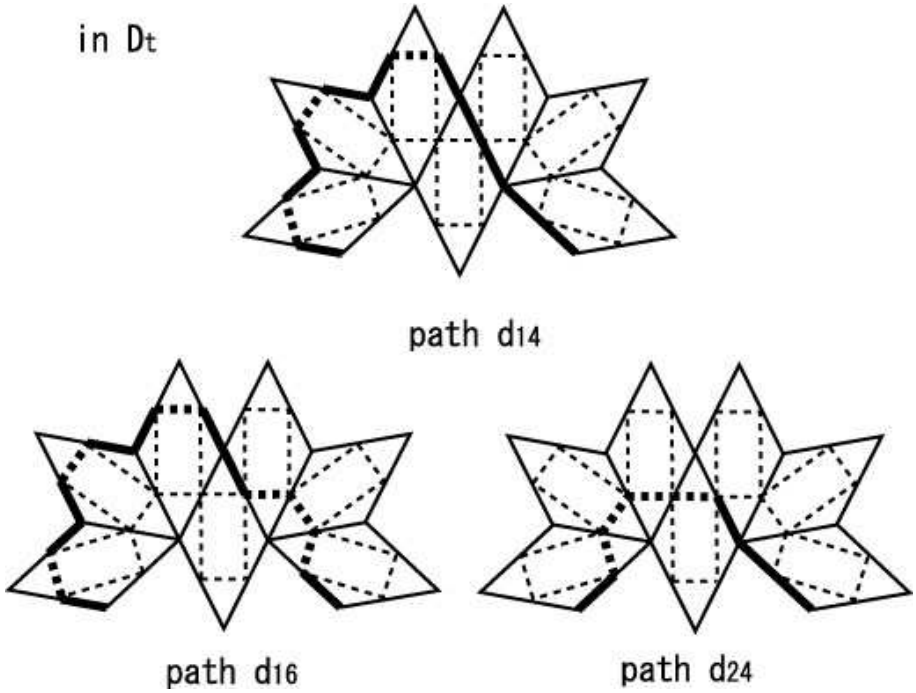

FIGURE 12.

$$E'_0 = f_0(E_0),\ f_0 = \begin{pmatrix} 1 & 0 \\ 2i-2 & 1 \end{pmatrix} \in G,\ -\frac{d}{c} = -\frac{1}{2i-2},$$
$$E'_1 = f_1(E_0),\ f_1 = \begin{pmatrix} 1 & 1 \\ 2i-2 & 2i-1 \end{pmatrix} \in G,\ -\frac{d}{c} = -\frac{2i-1}{2i-2},$$
$$E'_2 = f_2(E_0),\ f_2 = \begin{pmatrix} 1 & -1 \\ 2i & -(2i-1) \end{pmatrix} \in G,\ -\frac{d}{c} = \frac{2i-1}{2i}, \text{ and}$$
$$E'_3 = f_3(E_0),\ f_3 = \begin{pmatrix} 1 & 0 \\ 2i & 1 \end{pmatrix} \in G,\ -\frac{d}{c} = -\frac{1}{2i}$$

The first column $\begin{pmatrix} a_k \\ c_k \end{pmatrix}$ of f_k corresponds to the initial vertex a_k/c_k of the edge A_k, and the second column $\begin{pmatrix} b_k \\ d_k \end{pmatrix}$ of f_k corresponds to the initial vertex b_k/d_k of the edge B_k. The sign of each column is determined so that the determinant of f_k is equal to $+1$ rather than -1. Note that c_k is an even integer.

Hence, when $1 \leq t \leq \infty$ ($1 < t \leq \infty$ for C'_k), from Table 2.1, we obtain Table 4.1 of contribution to the intersection numbers i_1 and i_2 for the edges of the i-th quadrilateral in the first sequence of $Q_{p/q}$.

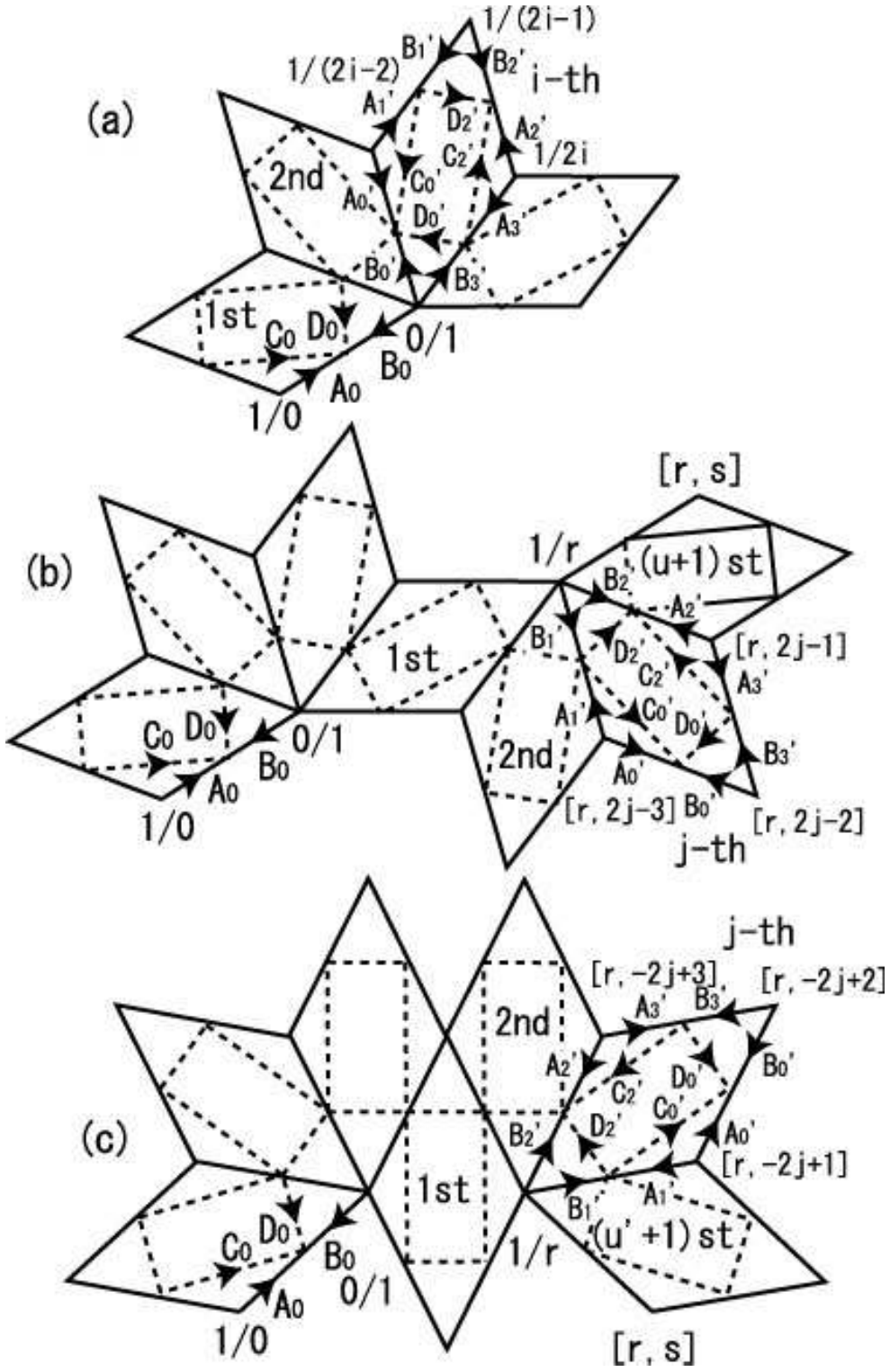
(a)
1/(2i−1)
1/(2i−2)
i−th
2nd
1st
1/2i
0/1
1/0
(b)
[r, s]
1/r
(u+1) st
1st
2nd
[r, 2j−1]
[r, 2j−3]
[r, 2j−2]
j−th
0/1
1/0
(c)
j−th
[r, −2j+3]
[r, −2j+2]
2nd
[r, −2j+1]
1st
(u′ +1) st
1/r
[r, s]
0/1
1/0

FIGURE 13.

	$i=1$			$i \geq 2$		
	$-\frac{d}{c}$	i_1	i_2	$-\frac{d}{c}$	i_1	i_2
A'_0	∞	0	0	$-$	β	β
B'_0	∞	0	0	$-$	$-(\alpha-\beta)$	0
C'_0	∞	0	2β	$-$	0	2β
D'_0	∞	0	$\alpha-\beta$	$-$	$-(\alpha-\beta)$	$\alpha-\beta$
A'_1	∞	0	0	$-$	β	β
B'_1	∞	0	0	$-$	$-(\alpha-\beta)$	0
A'_2	$\frac{1}{2}$	$-\beta$	$-\beta$	$\frac{1}{2} < -\frac{d}{c} < 1$	$-\beta$	$-\beta$
B'_2	$\frac{1}{2}$	$\alpha-\beta$	0	$\frac{1}{2} < -\frac{d}{c} < 1$	$\alpha-\beta$	0
C'_2	$\frac{1}{2}$	-2β	0	$\frac{1}{2} < -\frac{d}{c} < 1$	-2β	0
D'_2	$\frac{1}{2}$	0	$\alpha-\beta$	$\frac{1}{2} < -\frac{d}{c} < 1$	$\alpha-\beta$	$\alpha-\beta$
A'_3	$-$	β	β	$-$	β	β
B'_3	$-$	$-(\alpha-\beta)$	0	$-$	$-(\alpha-\beta)$	0

Table 4.1

When $t = 1$, a minimal edge-path contains an edge labeled C only in the $(w+1)$th quadrilateral of the first sequence of $Q_{p/q}$ (the first quadrilateral of the second sequence). In fact, such an edge-path is only c_2 and d_2. The transformation $\begin{pmatrix} 1 & 0 \\ r-1 & 1 \end{pmatrix}$ brings the edge C_0 to the edge C' oriented from $1/r$ to $0/1$. Table 4.2 is derived from Table 2.2, and shows contribution of C' to the intersection numbers i_1 and i_2. Note that $r \geq 3$.

	$-\frac{d}{c}$	i_1	i_2
C'	$-$	$2(\beta-n)$	$2n$

Table 4.2

For the j-th quadrilateral in the last sequence of quadrilaterals $Q_{p/q}$ with $s > 0$,

$$E'_0 = g_0(E_0),\ g_0 = \begin{pmatrix} -(2j-3) & 2j-2 \\ -\{(2j-3)r+1\} & (2j-2)r+1 \end{pmatrix} \in G,\ -\frac{d}{c} = \frac{(2j-2)r+1}{(2j-3)r+1},$$

$$E'_1 = g_1(E_0),\ g_1 = \begin{pmatrix} -(2j-3) & 1 \\ -\{(2j-3)r+1\} & r \end{pmatrix} \in G,\ -\frac{d}{c} = \frac{r}{(2j-3)r+1},$$

$$E'_2 = g_2(E_0),\ g_2 = \begin{pmatrix} 2j-1 & -1 \\ (2j-1)r+1 & -r \end{pmatrix} \in G,\ -\frac{d}{c} = \frac{r}{(2j-1)r+1}, \text{ and}$$

$$E'_3 = g_3(E_0),\ g_3 = \begin{pmatrix} 2j-1 & 2j-2 \\ (2j-1)r+1 & (2j-2)r+1 \end{pmatrix} \in G,\ -\frac{d}{c} = -\frac{(2j-2)r+1}{(2j-1)r+1}$$

Hence, when $1 \leq t \leq \infty$ ($1 < t \leq \infty$ for C'_k), we obtain Table 4.3 of contribution to the intersection numbers i_1 and i_2 for the edges of the j-th quadrilateral in the second sequence of $Q_{p/q}$ with $s > 0$. Note that the numbers of the table are independent of r.

	$j=1$			$j\geq 2$		
	$-\frac{d}{c}$	i_1	i_2	$-\frac{d}{c}$	i_1	i_2
A'_0	$-$	β	β	$1<-\frac{d}{c}<\infty$	$-\beta$	$-\beta$
B'_0	$-$	$-(\alpha-\beta)$	0	$1<-\frac{d}{c}<\infty$	$\alpha-\beta$	0
C'_0	$-$	0	2β	$1<-\frac{d}{c}<\infty$	0	2β
D'_0	$-$	$-(\alpha-\beta)$	$\alpha-\beta$	$1<-\frac{d}{c}<\infty$	$\alpha-\beta$	$\alpha-\beta$
A'_1	$-$	β	β	$0<-\frac{d}{c}<1$	$-\beta$	$-\beta$
B'_1	$-$	$-(\alpha-\beta)$	0	$0<-\frac{d}{c}<1$	$\alpha-\beta$	0
A'_2	$\frac{1}{2}<-\frac{d}{c}<1$	$-\beta$	$-\beta$	$0<-\frac{d}{c}<\frac{1}{2}$	$-\beta$	$-\beta$
B'_2	$\frac{1}{2}<-\frac{d}{c}<1$	$\alpha-\beta$	0	$0<-\frac{d}{c}<\frac{1}{2}$	$\alpha-\beta$	0
C'_2	$\frac{1}{2}<-\frac{d}{c}<1$	-2β	0	$0<-\frac{d}{c}<\frac{1}{2}$	-2β	0
D'_2	$\frac{1}{2}<-\frac{d}{c}<1$	$\alpha-\beta$	$\alpha-\beta$	$0<-\frac{d}{c}<\frac{1}{2}$	$-(\alpha-\beta)$	$\alpha-\beta$
A'_3	$-$	β	β	$-$	β	β
B'_3	$-$	$-(\alpha-\beta)$	0	$-$	$-(\alpha-\beta)$	0

Table 4.3

For the j-th quadrilateral in the last sequence of quadrilaterals $Q_{p/q}$ with $s<0$,

$$E'_0=h_0(E_0),\ h_0=\begin{pmatrix} -(-2j+1) & -2j+2 \\ -\{(-2j+1)r+1\} & (-2j+2)r+1 \end{pmatrix}\in G,\ -\frac{d}{c}=\frac{(-2j+2)r+1}{(-2j+1)r+1},$$

$$E'_1=h_1(E_0),\ h_1=\begin{pmatrix} -(-2j+1) & 1 \\ -\{(-2j+1)r+1\} & r \end{pmatrix}\in G,\ -\frac{d}{c}=\frac{r}{(-2j+1)r+1},$$

$$E'_2=h_2(E_0),\ h_2=\begin{pmatrix} -2j+3 & -1 \\ (-2j+3)r+1 & -r \end{pmatrix}\in G,\ -\frac{d}{c}=\frac{r}{(-2j+3)r+1},\text{ and}$$

$$E'_3=h_3(E_0),\ h_3=\begin{pmatrix} -2j+3 & -2j+2 \\ (-2j+3)r+1 & (-2j+2)r+1 \end{pmatrix}\in G,\ -\frac{d}{c}=-\frac{(-2j+2)r+1}{(-2j+3)r+1}$$

Hence, when $1\leq t\leq\infty$ ($1<t\leq\infty$ for C'_k), we obtain Table 4.4 of contribution to the intersection numbers i_1 and i_2 for the edges of the j-th quadrilateral in the second sequence of $Q_{p/q}$ with $s<0$. Note that the numbers of the table are independent of r.

	$j=1$			$j \geq 2$		
	$-\frac{d}{c}$	i_1	i_2	$-\frac{d}{c}$	i_1	i_2
A'_0	$-$	β	β	$\frac{1}{2} < -\frac{d}{c} < 1$	$-\beta$	$-\beta$
B'_0	$-$	$-(\alpha-\beta)$	0	$\frac{1}{2} < -\frac{d}{c} < 1$	$\alpha-\beta$	0
C'_0	$-$	0	2β	$\frac{1}{2} < -\frac{d}{c} < 1$	-2β	0
D'_0	$-$	$-(\alpha-\beta)$	$\alpha-\beta$	$\frac{1}{2} < -\frac{d}{c} < 1$	$\alpha-\beta$	$\alpha-\beta$
A'_1	$-$	β	β	$-$	β	β
B'_1	$-$	$-(\alpha-\beta)$	0	$-$	$-(\alpha-\beta)$	0
A'_2	$\frac{1}{2} < -\frac{d}{c} < 1$	$-\beta$	$-\beta$	$-$	β	β
B'_2	$\frac{1}{2} < -\frac{d}{c} < 1$	$\alpha-\beta$	0	$-$	$-(\alpha-\beta)$	0
C'_2	$\frac{1}{2} < -\frac{d}{c} < 1$	-2β	0	$-$	0	2β
D'_2	$\frac{1}{2} < -\frac{d}{c} < 1$	$\alpha-\beta$	$\alpha-\beta$	$-$	$-(\alpha-\beta)$	$\alpha-\beta$
A'_3	$0 < -\frac{d}{c} \leq \frac{1}{2}$	$-\beta$	$-\beta$	$-$	β	β
B'_3	$0 < -\frac{d}{c} \leq \frac{1}{2}$	$\alpha-\beta$	0	$-$	$-(\alpha-\beta)$	0

Table 4.4

5. Euler characteristic

We give a formula for the Euler characteristic $\chi(F)$ in this section. We consider only the case of $1 \leq t \leq \infty$. (In the case of $0 \leq t \leq 1$, we simply exchange α and β.)

Let $e_1, e_2, \cdots, e_k$ be the edges of the minimal edge-path. Let F_i be the part of F carried by Σ_{e_i}. Then $\chi(F) = (\Sigma_{i=1}^{k}\chi(F_i)) - (k-1)(\alpha+\beta)$ since F_i and F_{i+1} are glued together along $\alpha+\beta$ arcs. Each $\chi(F_i)$ is as in Table 5.1 according to the label of the edge e_i.

label	$\chi(\Sigma_{e_i})$
A	α
B	$2\beta + \frac{\alpha-\beta}{2}$
C	α
D	2β

Table 5.1

In fact, for the label A, F_i is a disjoint union of $(\alpha-\beta)+\beta = \alpha$ discs. For the label B, F_i is a disjoint union of $2\beta + \frac{\alpha-\beta}{2}$ discs. For the label C, F_i is a disjoint union of $(\alpha-\beta)+\beta = \alpha$ discs. For the label D, F_i is a disjoint union of 2β discs and 0 or more annuli (discs punctured by L_2). Precisely, F_i has α annuli when $\beta = 0$, and no annuli when $\beta \neq 0$. See Figures 14 and 15, where F_i with label D with $\alpha = 1, \beta = 0, n = 1$ and $\alpha = 2, \beta = 1, n = 1$ respectively are described.

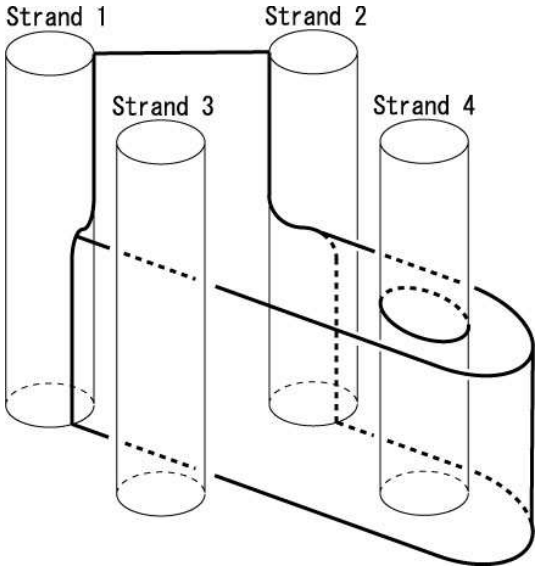

FIGURE 14.

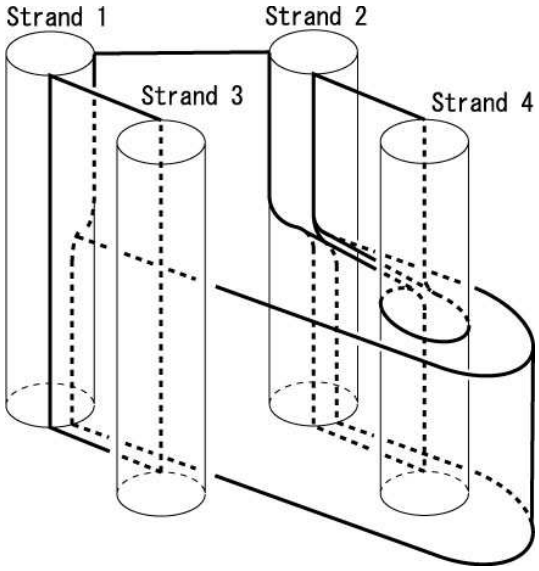

FIGURE 15.

6. Generalized genus

Let F be a compact 2-manifold. F may be orientable or non-orientable, and connected or disconnected. $g'(F)$ denotes the *generalized genus* defined by $\chi(F) = 2 - 2g'(F) - b(F)$, where $\chi(F)$ is the Euler characteristic of F, and $b(F)$ the number of boundary circles.

Lemma 6.1. *If $g'(F) = 0$, then F has a planar surface component or a projective plane with holes component.*

If $g'(F) = 1$, then F has either a planar surface component, a projective plane with holes component, a torus with holes component or a Klein bottle with holes component.

Proof. For a connected orientable surface F_0, the usual genus is calculated by $g(F_0) = \{2 - \chi(F_0) - b(F_0)\}/2$. Hence $b(F_0) \leq -\chi(F_0)$ when $g(F_0) \geq 1$, and $b(F_0) \leq -\chi(F_0) - 2$ when $g(F_0) \geq 2$.

For a connected non-orientable surface F_0, set $t(F_0) = 2-\chi(F_0)-b(F_0)$. Then $t(F_0) \geq 1$. F_0 is a projective plane (with holes) if $t(F_0) = 1$. F_0 is a Klein bottle (with holes) if $t(F_0) = 2$. Moreover, $b(F_0) \leq -\chi(F_0)$ when $t(F_0) \geq 2$, and $b(F_0) \leq -\chi(F_0) - 1$ when $t(F_0) \geq 3$.

The calculation below shows the latter half of this lemma. (The former half follows similarly.) Set $F = F_1 \cup ... \cup F_n$, where F_i is a connected component for $1 \leq i \leq n$. If $g(F_i) \geq 2$ for each orientable component F_i of F and if $t(F_j) \geq 3$ for each non-orientable component F_j, then $b(F) = \Sigma_k b(F_k) \leq \Sigma_k(-\chi(F_k) - 1) = -\chi(F) - n$. Then $g'(F) = \{2 - \chi(F) - b(F)\}/2 \geq \{2 + (b(F) + n) - b(F)\}/2 = (n + 2)/2 = n/2 + 1 > 1$. □

Remark 6.2. Let F be a compact 2-manifold properly embedded in an orientable 3-manifold M. Let $F_1, \cdots, F_n$ be orientable connected components of F, and $P_1, \cdots, P_m$ non-orientable ones. A regular neighbourhood $N(P_i)$ of each P_i is a twisted I-bundle over P_i. Let $\tilde{P}_i$ be the frontier surface of $N(P_i)$, that is, $\tilde{P}_i = \mathrm{cl}\,(\partial N(P_i) - \partial M)$, which is a connected orientable surface, and called the *double* of P_i in this paper. Then, an easy calculation shows $g'(F) = 1 + \Sigma_{i=1}^{n}(g(F_i) - 1) + \frac{1}{2}\Sigma_{j=1}^{m}(g(\tilde{P}_i) - 1)$.

Note that the double of a projective plane with holes is a planar surface, and that the double of a Klein bottle with holes is a torus with holes.

7. Surface 1-6 with $s > 0$ and $1 \leq t \leq \infty$

In this section, we calculate boundary slope of the surface F corresponding to the edge-path c_{16} with $s > 0$ and $1 \leq t \leq \infty$. We are going to obtain the slope of the preferred longitude by substituting 1 for α, and 0 for β.

Table 7.1 shows the calculation which uses Tables 4.1 and 4.3. We can find from the left side the columns of vertices, quadrilaterals, labels of edges, i_1, i_2 and $\chi(F_i)$. In the second column, the sign of $-A_2'$ means that the orientations of e_i and $g(A_0)$ don't match. In the 5–7th rows, $2 \leq i \leq w$. In the third row from the bottom, $2 \leq j \leq u + 1$.

Thus, from Table 7.1, the "slope" on $\partial N(L_1)$ is $(\alpha, (w - u)(\alpha - \beta) + (2w + 1)\beta)$ and that on $\partial N(L_2)$ is $(\beta, (w + u + 1)(\alpha - \beta) + (2w + 1)\beta)$, where the first coordinate is the longitudinal entry, and the second coordinate is the "meridional" entry with respect to the unusual longitude λ_1. To obtain the real slope, we need to know the "slope" of the preferred longitude, and divide the entries by their greatest common measure. $\partial F \cap \partial N(L_1)$ has $GCM(\alpha, (w-u)(\alpha-\beta)+(2w+1)\beta) = GCM(\alpha, (w-u)\alpha+(w+u+1)\beta) = GCM(\alpha, (w+$

$u+1)\beta)$ circles, and $\partial F \cap \partial N(L_2)$ has $GCM(\beta,(w+u+1)(\alpha-\beta)+(2w+1)\beta) = GCM(\beta,(w+u+1)\alpha+(w-u)\beta) = GCM(\beta,(w+u+1)(\alpha-\beta))$ circles.

Substituting 1 for α and 0 for β, we obtain the "slope" of the preferred longitude of L_1, which is $(1, w-u)$. In this case, the minimal edge-path is that of c_6 in D_∞, and is composed only of $w+u+1$ edges labeled D. The surface carried by Σ_D with $\alpha=1$ and $\beta=0$ is a disc punctured by L_2 once. See Figure 14. Hence F is a disc bounded by L_1 punctured by L_2 $w+u+1$ times.

Thus the slopes with respect to the preferred longitude can be obtained from $(\alpha,(w-u)\alpha+(w+u+1)\beta-(w-u)\alpha) = (\alpha,(w+u+1)\beta)$ on $\partial N(L_1)$, and $(\beta,(w+u+1)\alpha+(w-u)\beta-(w-u)\beta) = (\beta,(w+u+1)\alpha)$ on $\partial N(L_2)$ by dividing by the G.C.M. of the longitudinal entry and the meridional entry.

vertex	quadrilateral	label	i_1	i_2	$\chi(F_i)$
$\frac{1}{0}\sim$	$i=1$	A_1'	0	0	α
		D_2'	0	$\alpha-\beta$	2β
$\sim\frac{1}{2}$		$-A_2'$	β	β	α
$\frac{1}{2i-2}\sim$	$2\le i\le w$	A_1'	β	β	α
		D_2'	$\alpha-\beta$	$\alpha-\beta$	2β
$\sim\frac{1}{2i}$		$-A_2'$	β	β	α
$\frac{1}{r-1}\sim$	$i=w+1$	A_1'	β	β	α
		D_2'	$\alpha-\beta$	$\alpha-\beta$	2β
	$2\le j\le u+1$	D_2'	$-(\alpha-\beta)$	$\alpha-\beta$	2β
$\sim[r,s]$	$j=u+1$	$-A_2'$	β	β	α
	total	$\alpha-\beta$ entry	$w-u$	$w+u+1$	$2(w+1)$
		β entry	$2w+1$	$2w+1$	$2(2w+u+2)$

Table 7.1

We can calculate Euler characteristic by

$\chi(F) = 2(w+1)(\alpha-\beta)+2(2w+u+2)\beta-\{(3w+u+3)-1\}(\alpha+\beta) = -(w+u)(\alpha-\beta)-2w\beta.$

Thus the generalized genus is

$g'(F) = \{(w+u)(\alpha-\beta)+2w\beta-GCM(\alpha,(w+u+1)\beta)-GCM(\beta,(w+u+1)(\alpha-\beta))+2\}/2.$

8. Surface 2-6 with $s<0$ and $1<t\le\infty$

In this section, we calculate boundary slope of the surface F corresponding to the edge-path d_{26} with $s<0$ and $1<t\le\infty$. We set $s=2u+1=-(2u'+1)$. We are going to obtain the slope of the preferred longitude by substituting 1 for α, and 0 for β.

Table 8.1 shows the calculation which uses Tables 4.1 and 4.4. In the 3rd row, $2\le i\le w$. In the 5th row, $2\le j\le u'+1$.

Thus the "slope" on $\partial N(L_1)$ is $(\alpha, (w+u'-1)(\alpha-\beta)-\beta)$ and that on $\partial N(L_2)$ is $(\beta, -(w+u')(\alpha-\beta)-3\beta)$. $\partial F \cap \partial N(L_1)$ has $b_1 = GCM(\alpha, (w+u'-1)(\alpha-\beta)-\beta) = GCM(\alpha, (w+u')\beta)$ circles, and $\partial F \cap \partial N(L_2)$ has $b_2 = GCM(\beta, -(w+u')(\alpha-\beta)-3\beta) = GCM(\beta, (w+u')(\alpha-\beta))$ circles.

Substituting 1 for α and 0 for β, we obtain the "slope" of the preferred longitude of L_1, which is $(1, w+u'-1)$. In this case, F is a disc bounded by L_1 punctured by L_2 $w+u'$ times.

Thus the slopes with respect to the preferred longitude can be obtained from $(\alpha, (w+u'-1)(\alpha-\beta)-\beta-(w+u'-1)\alpha) = (\alpha, -(w+u')\beta)$ on $\partial N(L_1)$, and $(\beta, -(w+u')(\alpha-\beta)-3\beta-(w+u'-1)\beta) = (\beta, -(w+u')\alpha-2\beta)$ on $\partial N(L_2)$ by divided by the G.C.M. of the longitudinal entry and the meridional entry.

vertex	quadrilateral	label	i_1	i_2	$\chi(F_i)$
$\frac{1}{0} \sim$	$i=1$	A'_0	0	0	α
		$-D'_0$	0	$-(\alpha-\beta)$	2β
	$2 \le i \le w$	$-D'_0$	$\alpha-\beta$	$-(\alpha-\beta)$	2β
	$i = w+1$	$-C'_0$	0	-2β	α
	$2 \le j \le u'+1$	$-D'_2$	$\alpha-\beta$	$-(\alpha-\beta)$	2β
$\sim [r,s]$	$j = u'+1$	$-A'_1$	$-\beta$	$-\beta$	α
	total	$\alpha-\beta$ entry	$w+u'-1$	$-(w+u')$	3
		β entry	-1	-3	$2w+2u'+3$

Table 8.1

We can calculate Euler characteristic by
$\chi(F) = 3(\alpha-\beta) + (2w+2u'+3)\beta - \{(w+u'+3)-1\}(\alpha+\beta) = -(w+u'-1)(\alpha-\beta)-\beta.$

Thus the generalized genus is
$g'(F) = \{(w+u'-1)(\alpha-\beta)+\beta-b_1-b_2+2\}/2,$
where $b_1 = GCM(\alpha, (w+u')\beta)$ and $b_2 = GCM(\beta, (w+u')(\alpha-\beta))$.

9. DATA OF ALL THE ESSENTIAL SURFACES FOR $L([r,s])$

We can obtain boundary slopes, Euler characteristic, generalized genus of the surfaces corresponding to all the minimal paths as below by similar calculations as in previous two sections.

The boundary slopes below are with respect to the ordinary preferred longitudes, each of which is the boundary of a disc bounded by a component L_i and punctured by the other component L_j. But they are not divided by the G.C.M. of the longitudinal entry and the meridional entry.

For $L([r,s])$ with $s>0$, we obtain Tables 9.1 and 9.2 below, where c_2 is for $t=1$, c_{2k} is for $1 < t \le \infty$ and the others are for $1 \le t \le \infty$.

From data of c_{xy} with $x \neq 2$, we can obtain those for c_x by substituting β for α, and those for c_y by substituting 0 for β. We omit the data of the surfaces for $0 \leq t < 1$ because they are obtained from those for $1 \leq t \leq \infty$ by π-rotation of $L([r,s])$ about the axis $\Gamma(\frac{1}{2},\frac{1}{2}) \times \mathbb{R}$. We omit also the data of the surfaces corresponding to c_{38}, c_{36}, c_{28}, c_{27} since they are obtained from those for $L([s,r])$ corresponding to c_{14}, c_{16}, c_{24}, c_{25} by reflecting $L([s,r])$ upside down and transforming every level sphere by $\begin{pmatrix} s & -1 \\ sr+1 & -r \end{pmatrix}$.

path	slope on $\partial N(L_1)$	slope on $\partial N(L_2)$	Euler char.
c_2	$(\beta, -(w-u+1)\beta + 2n)$	$(\beta, -(w-u-1)\beta - 2n)$	$-\beta$
c_{14}	$(\alpha, (u+1)\alpha + w\beta)$	$(\beta, w\alpha + (u+1)\beta)$	$-w(\alpha+\beta)$
c_{16}	$(\alpha, (w+u+1)\beta)$	$(\beta, (w+u+1)\alpha)$	$-(w+u)(\alpha-\beta) - 2w\beta$
c_{24}	$(\alpha, (u+1)\alpha - w\beta)$	$(\beta, -w\alpha + (u-1)\beta)$	$-w(\alpha-\beta) - \beta$
c_{25}	$(\alpha, -(w-u-1)\alpha)$	$(\beta, -(w-u+1)\beta)$	$-\alpha$

Table 9.1

Let b_i be the number of boundary circles on $\partial N(L_i)$ for $i = 1$ and 2. Set $b = b_1 + b_2$.

path	generalized genus
c_2	$g' = (\beta - b + 2)/2, \quad b_1 = b_2 = GCM(\beta, 2n)$
c_{14}	$g' = \{w(\alpha+\beta) - b + 2\}/2, \quad b_1 = GCM(\alpha, w\beta), \ b_2 = GCM(\beta, w\alpha)$
c_{16}	$g' = \{(w+u)(\alpha-\beta) + 2w\beta - b + 2\}/2,$ $b_1 = GCM(\alpha, (w+u+1)\beta), \ b_2 = GCM(\beta, (w+u+1)\alpha)$
c_{24}	$g' = \{w(\alpha-\beta) + \beta - b + 2\}/2, \quad b_1 = GCM(\alpha, w\beta), \ b_2 = GCM(\beta, w\alpha)$
c_{25}	$g' = (-\beta + 2)/2, \quad (b_1 = \alpha, \ b_2 = \beta)$

Table 9.2

For $L([r,s])$ with $s < 0$, we obtain Tables 9.3 and 9.4 below, where d_2 is for $t = 1$, d_{2k} is for $1 < t \leq \infty$ and the others are for $1 \leq t \leq \infty$.

We omit also the data of the surfaces corresponding to d_{38}, d_{36}, d_{28} since they are obtained from those for $L([-s,-r])$ corresponding to d_{14}, d_{16}, d_{24} by π-rotating $L([-s,-r])$ about a horizontal line parallel to the x-axis and transforming every level sphere by $\begin{pmatrix} s & -1 \\ sr+1 & -r \end{pmatrix}$.

path	slope on $\partial N(L_1)$	slope on $\partial N(L_2)$	Euler char.
d_2	$(\beta, -(w-u+1)\beta+2n)$	$(\beta, -(w-u-1)\beta-2n)$	$-\beta$
d_{06}	$(\alpha, (w+u+1)\beta)$	$(\beta, (w-u-1)\alpha)$	$-(w-u-2)(\alpha+\beta)$
d_{14}	$(\alpha, (u+1)\alpha+w\beta)$	$(\beta, w\alpha+(u+1)\beta)$	$-w(\alpha+\beta)$
d_{16}	$(\alpha, (w+u+1)\beta)$	$(\beta, (w+u+1)\alpha)$	$-(w-u-2)(\alpha-\beta)-2w\beta$
d_{24}	$(\alpha, (u+1)\alpha-w\beta)$	$(\beta, -w\alpha+(u-1)\beta)$	$-w(\alpha-\beta)-\beta$
d_{25}	$(\alpha, -(w-u-1)\alpha)$	$(\beta, -(w-u+1)\beta)$	$-\alpha$
d_{26}	$(\alpha, -(w-u-1)\beta)$	$(\beta, -(w-u-1)\alpha-2\beta)$	$-(w-u-2)(\alpha-\beta)+\beta$
d_{27}	$(\alpha, -(w-u+1)\alpha)$	$(\beta, -(w-u-1)\beta)$	$-\alpha$

Table 9.3

path	generalized genus
d_2	$g'=(\beta-b+2)/2, \quad b_1=b_2=GCM(\beta,2n)$
d_{14}	$g'=\{w(\alpha+\beta)-b+2\}/2, \quad b_1=GCM(\alpha,w\beta),\ b_2=GCM(\beta,w\alpha)$
d_{06}	$g'=\{(w-u-2)(\alpha+\beta)-b+2\}/2,$ $b_1=GCM(\alpha,(w+u+1)\beta),\ b_2=GCM(\beta,(w-u-1)\alpha)$
d_{16}	$g'=\{(w-u-2)(\alpha-\beta)+2w\beta-b+2\}/2,$ $b_1=GCM(\alpha,(w+u+1)\beta),\ b_2=GCM(\beta,(w+u+1)\alpha)$
d_{24}	$g'=\{w(\alpha-\beta)+\beta-b+2\}/2, \quad b_1=GCM(\alpha,w\beta),\ b_2=GCM(\beta,w\alpha)$
d_{25}	$g'=(-\beta+2)/2, \quad (b_1=\alpha,\ b_2=\beta)$
d_{26}	$g'=\{(w-u-2)(\alpha-\beta)+\beta-b+2\}/2,$ $b_1=GCM(\alpha,(w-u-1)\beta),\ b_2=GCM(\beta,(w-u-1)\alpha)$
d_{27}	$g'=(-\beta+2)/2, \quad (b_1=\alpha,\ b_2=\beta)$

Table 9.4

10. Proof of necessity

We prove that, if $L([r,s])[\gamma_1,\gamma_2]$ is reducible, then the slopes γ_1,γ_2 are as in Theorem 1.2.

If a result of non-trivial Dehn surgery $L([r,s])[\gamma_1,\gamma_2]$ is reducible, then it is well-known that the exterior of $L([r,s])$ contains an incompressible and boundary incompressible planar surface P with non empty boundary circles of slope γ_i on $\partial N(L_i)$ for $i=1$ and 2. Because γ_1,γ_2 are non-meridional, the surface P is meridionally incompressible. Hence P is carried by a branched surface Σ_γ corresponding to a minimal edge-path γ in $Q_{[r,s]}$ as shown in [3]. So, we should know when generalized genus listed in the previous section can be zero. In fact, it can be zero only for $c_2, d_2, c_{25}, d_{25}, d_{26}$ and d_{27} by calculation as below.

Calculation for c_2 and d_2.

The generalized genus is zero only when $\beta=2$ and $n=0,1$ or 2 by the calculation below. Moreover, by Tables 9.1 and 9.3, we can calculate numbers of boundary circles and slopes. When $n=2$, 2 circles of slope $(1,-w+u+1)$ on $\partial N(L_1)$ and 2 circles of slope $(1,-w+u-1)$

on $\partial N(L_2)$, which is (1)(a) in Theorem 1.2. When $n = 1$, 2 circles of slope $(1, -w + u)$ both on $\partial N(L_1)$ and on $\partial N(L_2)$, which is (1)(b) in Theorem 1.2. When $n = 0$, 2 circles of slope $(1, -w + u - 1)$ on $\partial N(L_1)$ and 2 circles of slope $(1, -w + u + 1)$ on $\partial N(L_2)$, which is (1)(a) in Theorem 1.2.

$g' = \{\beta - 2GCM(\beta, 2n) + 2\}/2$ as in the lists. If $g' = 0$, then $\beta = 2GCM(\beta, 2n) - 2 = 2(GCM(\beta, 2n) - 1)$. Hence $\beta = 2\beta'$, for some positive integer β'. So, we have $\beta' = 2GCM(\beta', n) - 1 \cdots$ (i). Recall that $0 \le n \le \beta = 2\beta'$. If $GCM(\beta', n) \le \beta'/2$ then $\beta' = 2GCM(\beta', n) - 1 \le 2\frac{\beta'}{2} - 1 = \beta' - 1$, which is a contradiction. Hence $GCM(\beta', n) = \beta'$, and $\beta' = 1$ by (i).

Calculation for c_{25} and d_{25}.
The generalized genus $(-\beta + 2)/2$ is zero only when $\beta = 2$. Moreover, by Tables 9.1 and 9.3, the surface with $\beta = 2$ has α boundary circles of slope $(1, -w + u + 1)$ on $\partial N(L_1)$ and 2 boundary circles of slope $(1, -w + u - 1)$ on $\partial N(L_2)$, which is (1)(a) in Theorem 1.2.

Calculation for d_{27}.
The generalized genus $(-\beta + 2)/2$ is zero only when $\beta = 2$. Moreover, by Table 9.3, the surface with $\beta = 2$ has α boundary circles of slope $(1, -w + u - 1)$ on $\partial N(L_1)$ and 2 boundary circles of slope $(1, -w + u + 1)$ on $\partial N(L_2)$, which is (1)(a) in Theorem 1.2.

Lemma 10.1. *Let F be a surface properly embedded in the exterior of $L([r, s])$ such that the union of boundary circles ∂F goes around longitudinally α times on $\partial N(L_1)$ and β times on $\partial N(L_2)$. Suppose $\alpha \ge \beta > 0$. If the generalized genus g' of F is zero, then $\chi \ge -(\alpha+\beta)+2$, where χ is the Euler characteristics of F.*

Proof. Let b be the number of boundary circles of F. We have $b \le \alpha + \beta$. Recall $g' = \{-\chi - b + 2\}/2$. If $g' = 0$, then $\chi = -b + 2 \ge -(\alpha + \beta) + 2$. □

Calculations for $c_{14}, c_{16}, d_{14}, d_{06}, d_{16}$.
When $1 \le t < \infty$, Lemma 10.1 shows that generalized genera of the surfaces corresponding to $c_{14}, c_{16}, d_{14}, d_{06}, d_{16}$ are never zero. For example, the Euler characteristics of the surface corresponding to d_{16} is $-(w - u - 2)(\alpha - \beta) - 2w\beta \le -1 \cdot (\alpha - \beta) - 2 \cdot 1 \cdot \beta < -(\alpha + \beta) + 2$. Note that $u \le -2$ for d_{kl} since $s \le -3$.

When $t = \infty$, we have $\beta = 0$. The surface corresponding to c_4 or d_4 has $w\alpha$ boundary circles of meridional slope on $\partial N(L_2)$, and the surface corresponding to c_6 or d_6 has $(w+u+1)\alpha$ boundary circles of meridional slope on $\partial N(L_2)$. Since we are considering non-trivial Dehn surgery on $L([r, s])$, we can skip this case.

Calculation for d_{26}.
Generalized genus of the surface corresponding to d_{26} is zero only when $w = 1, u = -2, \alpha = 4, \beta = 2$. In this case, the surface has 4 boundary circles of slope $(1, -1)$ on $\partial N(L_1)$ and 2 boundary circles of slope $(1, -6)$ on $\partial N(L_2)$, which is (2) in Theorem 1.2. The calculation is a little harder. So, we give it in Appendix A.

Calculation for c_{24}, d_{24}.
Generalized genera of the surfaces corresponding to c_{24}, d_{24} are never zero. The calculation is similar to and much easier than that for d_{26}. So, we omit it.

11. Proof of sufficiency

In this section, we prove Theorems 1.3, 1.4 in section 1 and Theorem 11.1 below, which shows sufficiency of Theorem 1.2.

Let K be a knot in a 3-manifold M . K is called a *trivial knot* if it bounds a disc in M. K is called a *core knot* if its exterior $\mathrm{cl}\,(M - N(K))$ is a solid torus. K is called a *torus knot* if it is entirely contained in a Heegaard splitting torus of M. K is called a *cable knot* if it is isotoped in $\partial N(K')$ for some non-trivial non-core knot K' so that K winds 2 or more times longitudinally in the solid torus $N(K')$.

If we perform Dehn surgery of slope γ on one component of a 2-bridge link $L([r,s])$, then the other component forms a knot in a lens space, $S^1 \times S^2$ or S^3. We let $L([r,s])[\gamma]$ denote it. We assume that the surgery is performed on L_2 rather than L_1, following the proof of Theorem 5.1 in [13] by Wu.

Let L, M be the preferred longitude and the meridian of $N(L_2)$ before the Dehn surgery with the slope $+1$ being $L + M$. Let C' be a core circle of the exterior solid torus E of L_2 such that C' is homologous to M in E. We take M and L as a longitude and meridian system for $N(C')$, exchanging L and M. Let C be a core circle of the filled solid torus. We take M and γ as a longitude and meridian system for $N(C)$. Note that γ is eventually of integral slope in $N(L_2)$ in the next theorem.

Theorem 11.1. *Let w, u be integers with $w \geq 1$ and either $u \geq 1$ or $u \leq -2$. Then $L([2w+1, 2u+1])[\gamma]$ is a non-trivial non-core torus knot or a cable knot if and only if it is in one of the three cases below or its mirror image.*

1. *The knot $L([2w+1, 2u+1])[-w+u]$ is a torus knot in the $(-w+u, 1)$-lens space, which can be placed in $\partial N(L_2)$ so that it is a $(2w+1, -2)$-cable of C, and a $(2u+1, 2)$-cable of C'.*
2. *For some integer k, the knot $L([2w+1, 2u+1])[-w+u+\epsilon]$ with $\epsilon = \pm 1$ is a $(2, k)$-cable of a torus knot K in the $(-w+u+\epsilon, 1)$-lens space, where K can be placed in $\partial N(L_2)$ so that it is a $(\{(2u+1)+\epsilon\}/2, 1)$-cable of C', and a $(1, -\{(2w+1)-\epsilon\}/2)$-cable of C. Moreover, $L([2w+1, 2u+1])[-w+u+\epsilon]$ can be isotoped into $\partial N(L_2)$ to be two parallel copies of K except near a single $-\epsilon$ crossing. It is a cable knot, when $(w, \epsilon) \neq (1, 1)$ and $(u, \epsilon) \neq (1, -1), (-2, 1)$. When $(w, \epsilon) = (1, 1)$, $L([3, 2u+1])[u]$ is a torus knot which can be placed in $\partial N(L_2)$ so that it is a $(3, -2)$-cable of C, and a $(3u+2, 3)$-cable of C'. When $(u, \epsilon) = (-2, 1)$, $L([2w+1, -3])[-w-1]$ is a torus knot which can be placed in $\partial N(L_2)$ so that it is a $(3w+1, -3)$-cable of C, and a $(2, -3)$-cable of C'.*

(3) $L([3,-3])[-1]$ *is a trefoil knot in* S^3.

Necessity of Theorem 11.1 follows from that of Theorem 1.2. Conversely, sufficiency of Theorem 1.2 follows from that of Theorem 11.1 since a single Dehn surgery on a torus knot or a cable knot of a torus knot yields a reducible manifold. See [10] and [6].

Arguments similar to the proof of Theorem 5.1 in [13] show sufficiency of Theorem 11.1, 1.3 and 1.4. He found the case (2) there. The case (3) is well-known.

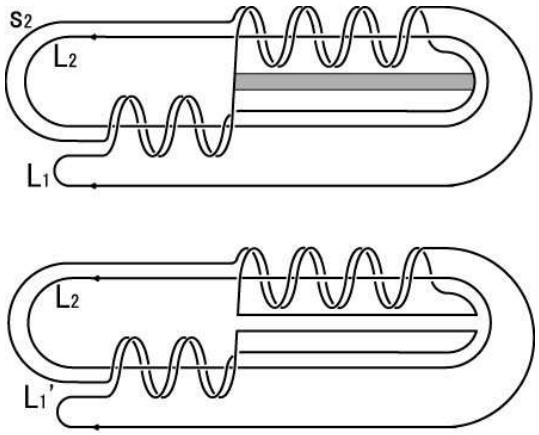

FIGURE 16.

Let $\cdot$ denote the algebraic intersection number on $\partial N(L_2)$ with $L \cdot M = +1$ rather than -1.

Proof. We prove Theorem 11.1 (1) and 1.3 (1).

$L([2w+1, 2u+1])[\infty, -w+u]$ is the 3-manifold obtained from S^3 by $(-w+u)$-Dehn surgery on the component L_2, and hence it is the $(-w+u, 1)$-lens space. It is again the 3-sphere when $-w+u = \pm 1$, and $S^2 \times S^1$ when $-w+u = 0$, because L_2 is the trivial knot.

Since a circle s_2 of the surgery slope $-w+u$ bounds a meridian disc of the Dehn filled solid torus, a band sum L_1' of L_1 and s_2 is isotopic to L_1 after the Dehn surgery in $L([2w+1, 2u+1])[\infty, -w+u]$. We consider the band as illustrated in Figure 16 (, where $w = 2, u = -4$ and s_2 is of slope $-w+u = -2-4 = -6$). For this band, L_1' can be embedded into the torus $\partial N(L_2)$ so that $L_1' = -2L - (2u+1)M$. It is a $(2, 2u+1)$-cable of the trivial knot L_2 in S^3, and a $(2u+1, 2)$-cable of the trivial knot C'. Note that $L_1' \cdot M = -2$ and $L_1' \cdot L = 2u+1$.

We can obtain the knot L_1' in $L([2w+1, 2u+1])[\infty, -w+u]$ by $(-w+u)$-Dehn surgery on L_2. The new meridian slope is $L + (-w+u)M$. Since $L_1' \cdot (L + (-w+u)M) = (-2L - (2u+1)M) \cdot (L + (-w+u)M) = -2(-w+u) + (2u+1) = 2w+1$ and $L_1' \cdot M = (-2L - (2u+1)M) \cdot M = -2$, and since $M \cdot (L + (-w+u)M) = -1$, L_1' is a $(2w+1, -2)$-cable of the core C of the filled solid torus.

We consider the case of $-w+u = \pm 1$, where $L([2w+1, 2u+1])[\infty, -w+u]$ is the 3-sphere. Set $\epsilon = L \cdot (L + (-w+u)M) = -w+u = \pm 1$, which is the algebraic intersection number of the meridian of $N(C')$ and that of $N(C)$. Hence L'_1 is the $(L'_1 \cdot (L+(-w+u)M), -\epsilon L'_1 \cdot L) = (2w+1, \mp(2u+1))$-torus knot. □

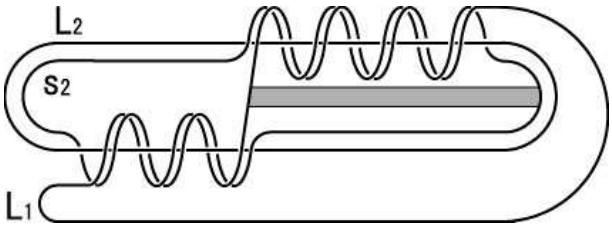

FIGURE 17.

Proof. We prove Theorem 11.1 (2), 1.3 (2) and 1.4. Similar argument as that for Theorem 11.1 (1) shows the former half of Theorem 11.1 (2).

The surgery slope is $-w+u+\epsilon$ with $\epsilon = \pm 1$. The band sum as in Figure 17 (,where $w = 2, u = -4$ and the surgery slope is $-w+u-1 = -2-4-1 = -7$,) gives the knot L'_1. For some integer m, the knot $L'_1 \subset S^3$ is a $(2,m)$-cable of a knot K in $\partial N(L_2)$, where $K = -L - \frac{(2u+1)+\epsilon}{2}M$. Hence K is a $(1, \{(2u+1)+\epsilon\}/2)$-cable of L_2, and a $(\{(2u+1)+\epsilon\}/2, 1)$-cable of C'. Note that $K \cdot L = \{(2u+1)+\epsilon\}/2$, and $K \cdot M = -1$.

As in Figure 17, L'_1 is the $(2, 2u+1)$-torus knot in S^3 before surgery if we ignore L_2, and hence L'_1 can be isotoped into the torus $\partial N(L_2)$ except near a single $-\epsilon$ crossing because $(2u+1) - 2\frac{(2u+1)+\epsilon}{2} = -\epsilon$.

After the Dehn surgery, $L + (-w+u+\epsilon)M$ is the new meridian slope of the filled solid torus. Hence K winds $K \cdot (L+(-w+u+\epsilon)M) = (-L - \frac{(2u+1)+\epsilon}{2}M) \cdot (L+(-w+u+\epsilon)M) = -(-w+u+\epsilon) + \{(2u+1)+\epsilon\}/2 = \{(2w+1)-\epsilon\}/2$ times longitudinally in the filled solid torus. Since $K \cdot M = -1$ and $M \cdot (L+(-w+u+\epsilon)M) = -1$, K is a $(1, -\{(2w+1)-\epsilon\}/2)$-cable of C.

$|\{(2u+1)+\epsilon\}/2|$ is never 0. It is equal to 1, if and only if $(u, \epsilon) = (1, -1)$ or $(-2, 1)$. $|\{(2w+1)-\epsilon\}/2|$ is never 0. It is equal to 1 if and only if $(w, \epsilon) = (1, 1)$. Hence the companion knot K is a core knot, when and only when $(w, \epsilon) = (1, 1)$ or $(u, \epsilon) = (1, -1), (-2, 1)$. (We consider these cases later.)

Otherwise, K is a non-trivial non-core torus knot, and L'_1 is a cable knot. When $-w+u+\epsilon = \sigma$ with $\sigma = \pm 1$, the surgery yields the 3-sphere. The case of $(\epsilon, \sigma) = (-1, -1), (-1, 1)$ are the mirror images of $(\epsilon, \sigma) = (1, 1), (1, -1)$ respectively with w and u exchanged. Hence we consider the case of $\epsilon = 1$ only. At this time, the new meridian of the filled solid torus is $L + \sigma M$, and $K = -L - (u+1)M$. The algebraic intersection number with the meridian L of C' is $L \cdot (L + \sigma M) = \sigma$. Since $K \cdot L = (-L - (u+1)M) \cdot L = u+1$ and

$K \cdot (L + \sigma M) = (-L - (u+1)M) \cdot (L + \sigma M) = (u+1) - \sigma$, K is the $(\sigma(u+1-\sigma), -(u+1)) = (\sigma(u+1)-1, -(u+1))$-torus knot in S^3. The slope of the cabling annulus of K is $-(\sigma(u+1)-1)(u+1) = -\sigma(u+1)^2+(u+1)$. Since L_1' has a single $-$ crossing in the diagram on $\partial N(L_2)$, L_1' is the $(2, 2\{-\sigma(u+1)^2 + (u+1)\} - 1) = (2, -2\sigma(u+1)^2 + 2u + 1)$-cable of K. Thus Theorem 1.4 follows.

We consider the case $(w, \epsilon) = (1, 1)$. (The case $(u, \epsilon) = (1, -1)$ is the mirror image of this case.) The surgery slope is $-w + u + \epsilon = u$. Recall that L_1' is on the boundary torus of the filled solid torus except near the $-$ crossing. We can move the knot L_1' entirely into the boundary torus by isotoping a very short under path near the crossing along a meridian disc of the filled solid torus. See Figure 18. Note that the algebraic intersection number between K and the new meridian is $(-L - \frac{(2u+1)+1}{2}M) \cdot (L + uM) = -u + \frac{(2u+1)+1}{2} = 1$ rather than -1. Hence L_1' is in the position of $2K - (L + uM) = 2(-L - \frac{(2u+1)+1}{2}M) - (L + uM) = -3L - (3u+2)M$. It is a $(3u+2, 3)$-cable of C'. Since $(-3L - (3u+2)M) \cdot (L + uM) = -3u + (3u+2) = 2$, $(-3L - (3u+2)M) \cdot M = -3$, and since $M \cdot (L + uM) = -1$, L_1' is a $(3, -2)$-cable of C. When $u = 1$, L_1' is a torus knot in S^3. At this time, the new meridian of the filled solid torus is $L + M$, $L_1' \cdot L = 5$, $L_1' \cdot (L + M) = 2$. Since $L \cdot (L + M) = +1$, L_1' is the $(2, -5)$-torus knot. Thus we obtain Theorem 1.3 (2).

We consider the case $(u, \epsilon) = (-2, 1)$. At this time, the surgery slope is $-w + u + 1 = -w - 1 (\leq -2)$. (Such a surgery never yields S^3.) Hence $K = -L - \frac{(2(-2)+1)+1}{2}M = -L + M$. L_1' is on the boundary torus of the filled solid torus except near the $-$ crossing. We can move the knot L_1' entirely into the boundary torus by isotoping a very short over path near the crossing along a meridian disc of the complementary solid torus. Note that the algebraic intersection number between K and the meridian L of C' is $(-L + M) \cdot L = -1$ rather than $+1$. Hence L_1' is in the position of $2K - L = 2(-L + M) - L = -3L + 2M$. It is a $(2, -3)$-cable of C'. Since $(-3L + 2M) \cdot (L + (-w-1)M) = -3(-w-1) - 2 = 3w + 1$, $(-3L + 2M) \cdot M = -3$, and since $M \cdot (L + (-w-1)M) = -1$, L_1' is a $(3w+1, -3)$-cable of C. □

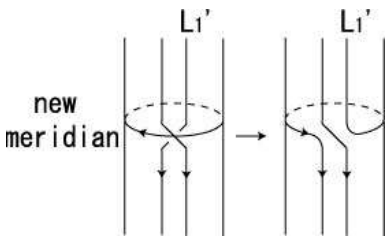

FIGURE 18.

12. Proof of Theorem1.6

The last sentence of Theorem 1.6 follows from Theorem 11.1. We prove the second sentence in this section.

Lemma 12.1. *Let F be a connected surface carried by a branched surface Σ_λ corresponding to a minimal edge-path λ for $L(p/q)$. Suppose that F has boundary circles on $\partial N(L_1)$ and does no circles on $\partial N(L_2)$. Then λ is composed of $2m$ edges of label B. The weights of F are $\alpha = 2$, $\beta = 0$, the slope of the boundary circles is integral, and the number of boundary circles is two. Moreover, $\chi(F) = -2m + 2$ and genus$(F) = m - 1$.*

Remark 12.2. In [12], Toshio Saito obtained a similar result to this lemma without using the result of Floyd and Hatcher.

Proof. Since F has not boundary circles on $\partial N(L_2)$, it cannot be partially carried by $\Sigma_A, \Sigma_C, \Sigma_D$, but only by Σ_B with $\beta = 0$ and $t = \infty$. Hence Σ_λ must be composed only of copies of Σ_B, and the corresponding minimal edge-path only of edges with label B.

Because the bottom arcs of Σ_B are loops, and since the top arc of Σ_B is a single arc, two consecutive copies of Σ_B in Σ_λ are glued along top arcs of both copies, or along bottom ones. Σ_B has a single branch locus which is the bottom arc of the square sector (the line of slope ∞) $\times[1/2, 1]$. We can split Σ_λ along the copies of the square sectors as above, so that it still carries F after the splittings. In fact, such splittings deform Σ_λ into a connected orientable surface Σ with no branch locus. Hence a surface carried by Σ_λ is the union of $\alpha/2$ parallel copies of Σ. Because F is connected, it is isotopic to Σ, and $\alpha = 2$. Since Σ forms a closed orientable surface when glued along L_1, the slope of the boundary circles is integral, and the number of boundary circles is two.

The top and the bottom of Σ_γ are copies of the top of Σ_γ because the bottom of Σ_γ is a union of loops. Hence Σ_λ consists of $2m$ copies of Σ_B for some positive integer m. Then $\chi(F) = 2m\frac{\alpha}{2} - (2m-1)\alpha = -2m+2$, and the genus is $\{-(-2m+2)-2+2\}/2 = m-1$. □

Proof. We prove the second sentence in Theorem 1.6. If $L(p/q)[\gamma]$ is a prime satellite knot, then its exterior contains an essential torus. We assume that the Dehn surgery is performed on L_1 rather than L_2. Then the exterior of the link contains an essential punctured torus T which has boundary circles only on $\partial N(L_1)$.

T is carried by a branched surface Σ_λ as in the conclusion of Lemma 12.1 with $m = 2$. Since $L(p/q) \cong L(p'/q')$ if $p/q - p'/q' \in \mathbb{Z}$, we can assume that the first edge is from $1/0$ to $0/1$. Thus $L(p/q) \cong L([2w, u, 2v])$ for some non-zero integers w, u, v. If $|w| = 1$ or $|v| = 1$, then λ is not minimal, which is a contradiction. If $|u| = 1$, then $L(p/q) \cong L([r, s])$ for some odd integers r, s.

For $L([r,s])$, minimal edge-paths composed only of edges of label B are c_5, c_7, d_5 or d_7. Substituting 0 for β in the expressions of the boundary slopes for the surfaces corresponding c_{25}, d_{25}, d_{27}, we obtain the desired slopes $(-w+u\pm 1, 1)$. □

Remark 12.3. The surface f_5 (resp. f_7) corresponding to c_5 or d_5 (resp. c_7 or d_7) with $\alpha = 2$ are obtained from the double of the surface f_2 corresponding to c_2 or d_2 with $\beta = 1$, $n = 1$ (resp. $n = 0$) by tubing operation on $\partial N(L_2)$ as shown in Figure 19. Note that the double of f_2 gives the cabling annulus when its boundary circles on $\partial N(L_1)$ are capped off with discs after the Dehn surgery.

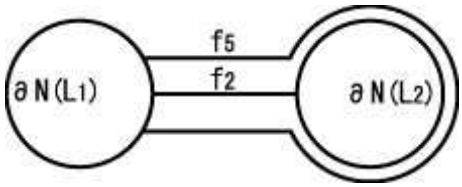

FIGURE 19.

A. CALCULATION FOR d_{26}

When $g' = 0$, we have the following three equations, where we set $m = w - u - 1 = w + u' (\geq 2)$.

$b_1 + b_2 = (m-1)(\alpha - \beta) + \beta + 2 \cdots$ (i)

$b_1 = GCM(\alpha, m\beta) = GCM(\alpha, m(\alpha - \beta)) \cdots$ (ii)

$b_2 = GCM(\beta, m\alpha) = GCM(\beta, m(\alpha - \beta)) \cdots$ (iii)

Since $1 < t \leq \infty$, it holds $\alpha > \beta \geq 0$. When $\beta = 0$, the surface has boundary circles of the meridional slope, which is not derived from non-trivial Dehn surgery. Hence we can assume $\alpha > \beta > 0$. Thus $b_1 = GCM(m\beta, \alpha)$ (resp. $b_2 = GCM(m\alpha, \beta)$) is exact divisor of α (resp. β) smaller than or equal to α (resp. β).

When $b_1 \leq \alpha/2$ and $b_2 \leq \beta/2$, we have $(\alpha+\beta)/2 \geq (m-1)(\alpha-\beta) + \beta + 2$ from (i). This implies $(\alpha+\beta)/2 \geq 1 \cdot (\alpha - \beta) + \beta + 2$ since $m \geq 2$. Then it follows $\beta - 4 \geq \alpha$, which contradicts $\alpha > \beta$. Hence we can assume that $b_1 = \alpha$ or $b_2 = \beta$.

The case of $b_1 = \alpha$.

Since $\alpha = b_1 = GCM(\alpha, m(\alpha - \beta))$, we can see that α is an exact divisor of $m(\alpha - \beta)$, and there is a positive integer k with $m(\alpha - \beta) = k\alpha \cdots$ (ii)′.

On the other hand, from (iii), there is a positive integer h with $hb_2 = m(\alpha - \beta) \cdots$ (iii)′. There are 2 cases, $h = 1$ and $h \geq 2$.

When $h = 1$, we have $b_2 = m(\alpha - \beta) \cdots$ (iii)″. In the equation (i), we substitute α for b_1 and $m(\alpha - \beta)$ for b_2, to obtain $\alpha - \beta = 1$. Then $b_2 = m$ from (iii)″, $m = k\alpha$ from (ii)′. So,

again from (iii), $m = b_2 = GCM(\beta, m(\alpha - \beta))$, which implies that m is an exact divisor of β and $m \leq \beta$. Thus $\beta \geq m = k\alpha \geq \alpha$, contradicting to $\alpha > \beta$. This implies that $h = 1$ is inadequate.

Hence we can assume $h \geq 2$. Substituting α for b_1 and $\frac{m(\alpha-\beta)}{h}$ for b_2 in the equation (i), we obtain $(m\frac{h-1}{h} - 2)(\alpha - \beta) = -2 \cdots$ (i)$'$. Comparing signs of both sides, we can see $m\frac{h-1}{h} - 2 < 0$, and a short calculation gives $m < \frac{2h}{h-1} (\leq 4)$. Since $h \geq 2$ and $m \geq 2$, either $m = 2$, or $h = 2$ and $m = 3$.

We first consider the case of $m = 2$. Substituting 2 for m in (i)$'$, we obtain $\alpha - \beta = h \cdots$ (i)$''$. Hence, from (iii)$'$, $b_2 = m = 2 \cdots$ (iii)$'''$. From (ii), $\alpha = b_1 = GCM(\alpha, 2\beta)$, which implies that there is a positive integer v with $v\alpha = 2\beta$. Substituting $\beta + h$ for α by (i)$''$, we obtain $(2 - v)\beta = hv$. Hence $2 - v > 0$, which implies $v = 1$ and $\beta = h$. Then $\alpha = 2h$ from (i)$''$. From (iii) and (iii)$'''$, $2 = b_2 = GCM(\beta, m\alpha) = GCM(h, 2 \cdot 2h) = h$. Thus we have $\alpha = 4,\ \beta = 2,\ w + u' = m = 2$, which is the unique solution of the equations for d_{26}.

We consider the case where $h = 2$ and $m = 3$. In this case, we obtain from (i)$'$ $\alpha - \beta = 4 \cdots$ (i)$'''$. Hence, from (iii)$'$, $b_2 = 6$. Then, from (iii), $6 = b_2 = GCM(\beta, 12)$, which implies that β is a multiple of 6. From (ii), $\alpha = b_1 = GCM(\alpha, 12)$. This implies α is an exact divisor of 12. Hence $\alpha = 12$ and $\beta = 6$ because $12 \geq \alpha > \beta \geq 6$. This contradicts (i)$'''$.

The case of $b_2 = \beta$.

The equation (ii) implies that there is a positive integer h with $hb_1 = m(\alpha - \beta) \cdots$ (ii)*.

We first consider the case of $h \geq 2$. Substituting β for b_2 and $\frac{m(\alpha-\beta)}{h}$ for b_1 in the equation (i), we obtain $(m\frac{h-1}{h} - 1)(\alpha - \beta) = -2$. Comparing signs of both sides, we can see $m\frac{h-1}{h} - 1 < 0$. Hence $m < \frac{h}{h-1} \leq 2$, which contradicts $m \geq 2$.

Hence we can assume $h = 1$. Then $b_1 = m(\alpha - \beta)$ from (ii)*. Substituting β for b_2 and $m(\alpha - \beta)$ for b_1 in (i), we obtain $\alpha - \beta = 2 \cdots$ (i)*. Then $b_1 = 2m$ again from (i). From (ii), $2m = b_1 = GCM(\alpha, m(\alpha - \beta))$, and hence there is a positive integer k with $\alpha = 2mk \cdots$ (ii)**. Substituting $\beta + 2$ for α by (i)*, we have $\beta + 2 = 2mk \cdots$ (ii)***. Then from (iii), $\beta = b_2 = GCM(2mk - 2, 2m) = GCM(2, 2m)$, which implies either $\beta = 1$ or $\beta = 2$. $\beta = 1$ contradicts (ii)***, and hence $\beta = 2$. Thus $\alpha = 4$ from (i)*, and $m = 2$ from (ii)** and $m \geq 2$. This is the unique solution for the equations for d_{26}.

References

1. M. Ait Nouh and A. Yasuhara, *Torus knots that cannot be untied by twisting*, Rev. Mat. Complut. 14 (2001), 423–437.
2. M. Brittenham and Y.-Q. Wu, *The classification of exceptional Dehn surgeries on 2-bridge knots*, Comm. Anal. Geom. 9 (2001), 97–113.
3. W. Floyd and A. Hatcher, *The space of incompressible surfaces in a 2-bridge link complement*, Trans. Amer. Math. Soc. 305 (1988), 575–599.
4. D. Gabai and U. Oertel, *Essential laminations in 3-manifolds*, Ann. of Math. (2) 130 (1989), 41–73.

5. H. Goda, C. Hayashi and H. Song, *A criterion for satellite* 1*-genus* 1*-bridge knots*, Proc. Amer. Math. Soc. 132 (2004), 3449–3456.
6. C. McA. Gordon, *Dehn surgery and satellite knots*, Trans. Amer. Math. Soc. 275 (1983), 687–708.
7. A. Hatcher and W. Thurston, *Incompressible surfaces in* 2*-bridge knot complements*, Invent. Math. 79 (1985), 225–246.
8. J. Hoste and P. D. Shanahan, *Computing boundary slopes of 2-bridge links*, preprint, available at http://front.math.ucdavis.edu/math.GT/0505442.
9. A. Lash, *Boundary curve space of the Whitehead link complement*, Dissertation, University of California, Santa Barbara (1993).
10. L. Moser, *Elementary surgery along a torus knot*, Pacific J. Math. 38 (1971), 737–745.
11. R. Patton, *Incompressible punctured tori in the complements of alternating knots*, Math. Ann. 301 (1995), 1–22.
12. T. Saito, *Satellite (1,1)-knots and meridionally incompressible surfaces*, Topology Appl. 149 (2005), 33–56.
13. Y.-Q. Wu, *Dehn surgery on Arborescent links*, Trans. Amer. Math. Soc. 351 (1999), 2275–2294.

Hiroshi Goda: Department of Mathematics, Tokyo University of Agriculture and Technology, Koganei, Tokyo, 184-8588, Japan. goda@cc.tuat.ac.jp

Chuichiro Hayashi: Department of Mathematical and Physical Sciences, Faculty of Science, Japan Women's University, 2-8-1 Mejirodai, Bunkyo-ku, Tokyo, 112-8681, Japan. hayashic@fc.jwu.ac.jp

Hyun-Jong Song: Division of Mathematical Sciences, Pukyong National University, 599-1 Daeyondong, Namgu, Pusan 608-737, Korea. hjsong@pknu.ac.kr